https://doi.org/10.5194/egusphere-2026-2146
Preprint. Discussion started: 4 May 2026


# Study on the influence of ENSO on total columns of ozone over the Tibetan Plateau

Haoyue Wang[1,2,★], Feihong Xiao[1,★], Ke Yu[1,3], Jianchun Bian[4,5,6], Dan Li[5], Qianyu Liu[1]

[1]Department of Atmospheric Sciences, Yunnan University, Kunming 650500, China
[2]Shanghai Key Laboratory of Atmospheric Particle Pollution and Prevention (LAP3), Department of Environmental Science and Engineering, Fudan University, Shanghai 200433, China
[3]Yunnan Meteorological Observatory, Kunming 650032, China
[4]College of Atmospheric Sciences, Lanzhou University, Lanzhou, China
[5]Key Laboratory of Middle Atmosphere and Global Environment Observation (LAGEO), Institute of Atmospheric Physics, Chinese Academy of Sciences, Beijing, China
[6]College of Earth and Planetary Sciences, University of Chinese Academy of Sciences, Beijing, China

★These authors contributed equally to this work.

Correspondence to: Haoyue Wang (wanghaoyue22@ynu.edu.cn)

**Abstract.**The El Niño-Southern Oscillation (ENSO) and the distinctive topographic features of the Tibetan Plateau (TP) exert a significant influence on the stratosphere-to-troposphere transport (STT) process. Their combined effects further amplify the spatiotemporal variability of tropospheric ozone ($O_3$) concentrations. To investigate the impact of ENSO on total column ozone (TCO) over the TP and the underlying mechanisms, this study employs the Weather Research and Forecasting Model with Chemistry (WRF-Chem). Results demonstrate that the single-synthesis simulation using WRF-Chem outperforms the multi-year simulation of the Whole Atmosphere Community Climate Model (WACCM) in capturing tropospheric TCO, zonal wind, potential height, and temperature. Over the TP, except in autumn, the variations in TCO within the lower stratosphere and troposphere exhibit opposite phases during El Niño and La Niña years. Specifically, TCO in the lower stratosphere is primarily regulated by the Brewer-Dobson circulation (BDC) and potential height. In contrast, TCO in the troposphere is shaped not only by potential height but also by STT processes and regional vertical circulation. The thermal effect of the TP plays a pivotal role in modulating the subtropical jet stream (STJ), potential height, and vertical circulation—with notable phase reversals observed between El Niño and La Niña years. Furthermore, the thermal effect of the TP acts in synergy with the Hadley Circulation (HC) to drive changes in the STJ, thereby exerting a significant impact on the spatiotemporal distribution of tropospheric $O_3$ over the TP.

**Short summary:**

This study employed atmospheric modeling simulations to demonstrate that El Niño-Southern Oscillation events modulate spatial distribution patterns and temporal trends of ozone over the Tibetan Plateau. This modulation occurs primarily through alterations in atmospheric wind fields, circulation systems, and the region's distinctive thermal forcing mechanisms.

https://doi.org/10.5194/egusphere-2026-2146
Preprint. Discussion started: 4 May 2026


## 1 Introduction

Ozone ($O_3$) in the atmosphere is predominantly concentrated in the stratosphere, with peak concentrations occurring at an altitude range of approximately 20–30 kilometers. In contrast, tropospheric $O_3$ accounts for only ~10% of the total atmospheric ozone burden. While stratospheric $O_3$ plays a pivotal role in shielding life on Earth from harmful ultraviolet (UV) radiation (WMO, 2022), elevated tropospheric $O_3$ concentrations are recognized as a significant air pollutant, posing substantial risks to human health and terrestrial ecosystems (Cooper, 2019). Tropospheric $O_3$ is primarily generated via photochemical reactions (Chen et al., 2024), but it is also modulated by stratosphere-troposphere exchange (STE) processes (Danielsen et al., 1977; Ding et al., 2006). STE comprises two core processes: stratosphere-to-troposphere transport (STT, i.e., the transport of ozone from the stratosphere to the troposphere) and troposphere-to-stratosphere transport (TST, i.e., the transport of ozone from the troposphere to the stratosphere). The occurrence and intensity of STE are regulated by multiple dynamical factors, including the secondary circulation associated with jet streams (Akritidis et al., 2018), the formation of upper-tropospheric/lower-stratospheric (UTLS) troughs, and the development of cut-off low-pressure systems (Li & Bian, 2018).

Previous studies have shown that STT exerts a significant influence on tropospheric $O_3$ concentrations in the midlatitudes of the Northern Hemisphere (Cristofanelli et al., 2010), with particularly notable impacts at high elevations (Bracci et al., 2012; Yin et al., 2017). Stratospheric $O_3$ can be transported downward into the troposphere; under favorable atmospheric circulation and meteorological conditions, this $O_3$ can be further mixed down to the surface. This process alters surface $O_3$ levels and directly impacts air quality (Schneidemesser et al., 2015; Wang et al., 2020; Zhang et al., 2022). The Tibetan Plateau (TP) is widely recognized as one of the global hotspots for STT (Yin et al., 2023). STT processes over the TP are modulated by strong land-sea thermal contrasts, as well as the thermal and dynamical forcing of the plateau itself. These factors give rise to distinct regional characteristics of STT over the TP, which in turn makes important contributions to hemispheric and even global STT. Consequently, the role of STT over the TP in regulating surface $O_3$ concentrations cannot be overlooked.

The El Niño–Southern Oscillation (ENSO) is a major tropical ocean–atmosphere anomaly that can induce global climate perturbations by propagating atmospheric teleconnections (Timmermann et al., 2018). While numerous studies have explored the influence of STT on tropospheric $O_3$ and its underlying mechanisms, recent evidence suggests that ENSO can also substantially modulate STT and the associated stratospheric $O_3$ influx into the troposphere (Bruckner et al., 2024). Specifically, ENSO affects both the location and intensity of STT by altering the position and strength of the jet stream (Langford, 1999; Luo et al., 2019). Additionally, it further impacts lower stratospheric $O_3$ by regulating the Brewer–Dobson circulation (BDC)—a process that, in turn, modifies the amount of stratospheric $O_3$ transferred to the troposphere during STT events (Albers et al., 2018). Given that ENSO drives global-scale climate anomalies, many studies have utilized global models for simulations (Albers et al., 2022; Lee et al., 2025). Although such models are effective for investigating global climate variability and long-term trends, they suffer from limitations including coarse spatial resolution and significant

https://doi.org/10.5194/egusphere-2026-2146
Preprint. Discussion started: 4 May 2026


regional biases (Chen et al., 2012; Kendon et al., 2014; Wang et al., 2024). To address these constraints, the present study employs the Weather Research and Forecasting model coupled with Chemistry (WRF-Chem) to examine the influence of ENSO on STT processes over the TP.

This study focuses on the TP—a region characterized by unique atmospheric circulation patterns.As the "Asian water tower," the TP plays a critical role in regulating regional ecology and climate. Notably, variations in tropospheric $O_3$ over the TP not only directly affect the local environment but also exhibit close links to STT processes. Despite ENSO being the most prominent global air–sea coupled phenomenon,the mechanisms by which ENSO modulates STT over the TP and the subsequent impacts on tropospheric $O_3$ remain poorly understood. Key knowledge gaps include: (1) differences in STT intensity and pathways under distinct ENSO phases (i.e., El Niño vs. La Niña) and (2) the quantitative relationship between STT and tropospheric $O_3$ concentrations. To address these gaps, this study aims to elucidate the physicochemical processes through which ENSO—driven by anomalous equatorial PacificSSTs—exerts remote effects on atmospheric circulation over the TP. These circulation anomalies, in turn, alter the efficiency and pathways of STT, ultimately leading to spatiotemporal variations in tropospheric $O_3$. Furthermore, by quantifying the relative contributions of lower stratospheric $O_3$ and STT frequency to tropospheric $O_3$ levels over the TP, this work clarifies the role of ENSO in modulating regional $O_3$ dynamics and reveals potential regulatory mechanisms. Importantly, this study represents the first application of the WRF-Chem to simulate these processes over the TP, enabling a detailed analysis of the STT response to ENSO and its associated impacts on tropospheric $O_3$.

## 2 Data and methods

### 2.1 Reanalysis and model data

In this study, the fifth-generation ECMWF Reanalysis (ERA5) dataset—developed by the European Centre for Medium-Range Weather Forecasts (ECMWF)—is utilized for two key purposes: driving simulations of the WRF-Chem and evaluating the resulting simulation outputs. ERA5 integrates physical model constraints with global observational data to produce a globally complete and internally consistent dataset, with a temporal coverage spanning from 1940 to the present. This dataset provides hourly observations of multiple atmospheric variables, including global wind fields, temperature, ozone ($O_3$), and relative humidity, all of which are available at various isobaric surfaces. In terms of spatial and vertical resolution, ERA5 features a horizontal resolution of 0.25° × 0.25° and a vertical domain consisting of 37 layers, ranging from the Earth's surface up to the 1 hPa pressure level.

To further assess the reliability of the WRF-Chem simulations, outputs from the Whole Atmosphere Community Climate Model (WACCM)—developed by the National Center for Atmospheric Research (NCAR)—were also utilized. WACCM provides global atmospheric fields with three temporal resolutions: three-hourly, 5-day averaged, and monthly averaged. These fields include key variables such as wind, temperature, and $O_3$, covering a vertical range from the Earth's surface up to

https://doi.org/10.5194/egusphere-2026-2146
Preprint. Discussion started: 4 May 2026


approximately 4–10 hPa and resolved across 145 vertical layers. Owing to its comprehensive coverage of stratospheric domains and high vertical resolution, this dataset is particularly well-suited for studies focusing on stratospheric processes and $O_3$ dynamics (Zhang et al., 2021; Thurairajah and Cullens, 2022; Wang et al., 2024).

### 2.2 The definition of ENSO

To investigate the influence of the ENSO on STT events over the TP, the Niño-3.4 sea surface temperature (SST) anomaly index—provided by the Climate Prediction Center (CPC)—was used to identify El Niño and La Niña years within the 2001–2020 period. Specifically, ENSO years were determined by calculating the average of SST anomalies over five consecutive autumn and winter months, with a threshold of ±0.5 °C (i.e., El Niño for ≥0.5 °C and La Niña for ≤−0.5 °C). Previous studies have demonstrated that STE-related $O_3$ exhibits a positive correlation with ENSO, and this $O_3$ response typically lags behind ENSO by approximately six months (Zeng & Pyle, 2005; Koumoutsaris et al., 2008; Voulgarakis et al., 2011). Furthermore, ENSO exerts impacts on East Asia through anomalous circulation in the Northwest Pacific, and this influence also shows a similar lag effect (Wang et al., 2000; Wie et al., 2021). In light of these findings, the present study defines the year following the ENSO event (as identified by the Niño-3.4 index) as the "ENSO event impact year" for analyzing STT and tropospheric $O_3$ variations over the TP.

Given the close linkage between Indian Ocean SST and the ENSO, anomalously warm conditions in the central and eastern Pacific are often accompanied by positive SST anomalies in the Indian Ocean (Yulaeva & Wallace, 1994; Enfield & Mayer, 1997; Kug & Kang, 2006). To minimize potential confounding effects of Indian Ocean variability on STT events over the TP, strong events associated with the Indian Ocean Dipole (IOD)—where the IOD index exceeds ±1.0—were excluded from the composite analysis. The IOD index is formally defined as the SST difference between two key regions: the western Indian Ocean (10° S–10° N, 50° E–70° E) and the eastern Indian Ocean (10° S–equator, 90° E–110° E). Specifically, positive IOD phases correspond to index values above +0.4, while negative phases correspond to values below −0.4; values exceeding ±1.0 are classified as strong IOD events. Indian Ocean SST data used in this study were obtained from the HadSST dataset developed by the Met Office Hadley Centre. After applying the aforementioned criteria (i.e., excluding strong IOD events), four El Niño events and six La Niña events were identified within the study period. Among these, one strong El Niño event and two strong La Niña events were further categorized—defined as events where the five-month average of the Niño-3.4 SST anomaly exceeds +1.0 or falls below −1.0, respectively (see Table 1).

**Table 1 the years affected by different phases of ENSO**

| El Niño | | La Niña | |
|---|---|---|---|
| Years | The Niño-3.4 index average(Oct-Feb) | Years | The Niño-3.4 index average(Oct-Feb) |

https://doi.org/10.5194/egusphere-2026-2146
Preprint. Discussion started: 4 May 2026


| | | | |
|---|---|---|---|
| 2003 | 1.07 | 2001 | -0.75 |
| 2005 | 0.63 | 2008 | -1.57 |
| 2007 | 0.73 | 2009 | -0.67 |
| 2015 | 0.57 | 2011 | -1.52 |
| | | 2012 | -0.97 |
| | | 2018 | -0.85 |

### 2.3 Patterns and simulation methods

In this study, the WRF-Chem V4.1.5 is employed to investigate the influence of the ENSO on STT events over the Tibetan Plateau (TP), as well as the underlying mechanisms. Previous studies have successfully applied both the Weather Research and Forecasting (WRF) model and its chemistry-coupled variant (WRF-Chem) to examine ENSO-related atmospheric and chemical phenomena (Evans and McCabe, 2010; Ratna et al., 2014; Xi and Sokolik, 2016; Manciu et al., 2023). Specifically, WRF is a mesoscale numerical weather prediction model jointly developed by the National Center for Atmospheric Research (NCAR), the National Centers for Environmental Prediction (NCEP) under the National Oceanic and Atmospheric Administration (NOAA), and other collaborating institutions. WRF-Chem, building on the WRF/Advanced Research WRF (ARW) framework, integrates an online chemistry module to simulate atmospheric chemical transport, transformation, and interactions (Grell et al., 2005). The initial and boundary conditions for both chemistry and meteorology in the WRF-Chem simulations were obtained from the Community Atmosphere Model with Chemistry (CAM-Chem) (Buchholz et al., 2019). Since the CAM-Chem boundary dataset is only available for the 2001–2020 period, this study restricts its focus exclusively to ENSO events occurring within this time frame.

In this study, the WRF-Chem simulations are driven by the ERA5 dataset—consistent with the dataset introduced earlier for model evaluation. Specifically, ERA5 provides six-hourly atmospheric fields with a horizontal resolution of 0.25° × 0.25°, which serve as the meteorological forcing for the simulations. For emission sources, anthropogenic emissions are prescribed using the Emissions Database for Global Atmospheric Research (EDGAR) Version 8.1, a widely used global anthropogenic emission inventory. In contrast, biogenic emissions are derived from the Model of Emissions of Gases and Aerosols from Nature (MEGAN), which quantifies natural emissions of trace gases and aerosols based on ecological and environmental factors. Together, these two emission datasets ensure comprehensive coverage of both human-induced and naturally occurring atmospheric emissions in the WRF-Chem simulations.

Following the method proposed by Kawase et al. (2009)—who using synthetic simulations, he assessed the impacts of climate warming on variations in the Baiu rainband, and demonstrated that the multi-year average of simulation results can be approximated by a single synthetic simulation, thereby substantially reducing computational costs—this study conducted synthetic simulations for three scenarios: El Niño, La Niña, and climatological states. This is the first known application of

https://doi.org/10.5194/egusphere-2026-2146
Preprint. Discussion started: 4 May 2026


this approach to investigate ENSO-associated TCO variations. These scenarios correspond to the ENSO events and time frame listed in Table 1. Specifically, to generate representative initial conditions for each scenario: (1) initial fields from the 4 identified El Niño years were averaged; (2) initial fields from the 6 identified La Niña years were averaged; and (3) initial fields from the full climatological period (2001 – 2020, 20 years) were averaged. Each synthetic simulation was integrated for 14 months, with the first 2 months treated as the model spin-up period and excluded from subsequent analysis to ensure the model reaches a stable state. To quantify the transport of stratospheric $O_3$, a passive stratospheric tracer was released at each time step of the simulations. This tracer exhibits three key properties: it does not participate in atmospheric chemical reactions, has no external sources or sinks, and its spatial distribution is solely governed by atmospheric transport processes. The spatiotemporal variations of this passive tracer in the troposphere were then used to assess the relative influence of ENSO on tropospheric $O_3$ concentrations over the TP.

During El Niño years, both the WACCM and the WRF-Chem successfully reproduce the variations in stratospheric $O_3$. Specifically, correlation coefficients between simulated and observed stratospheric $O_3$ exceed 0.95 in most seasons, while root mean square errors (RMSE) remain below 0.3 DU. In contrast, tropospheric $O_3$ exhibits greater variability in simulation performance across the two models. For tropospheric $O_3$, correlation coefficients range from 0.2 to 0.95, and RMSE values fall between 0.3 DU and 1.2 DU. When comparing the two models, WRF-Chem outperforms WACCM in simulating tropospheric $O_3$ during spring and winter, shows slightly lower accuracy in autumn, and achieves comparable performance to WACCM in summer (see Fig. 1a).

Consistent with the performance during El Niño years, both models (WACCM and WRF-Chem) also captured the variations in stratospheric $O_3$ well for La Niña years and the climatological state. For La Niña years: WRF-Chem simulations of stratospheric $O_3$ yielded correlation coefficients greater than 0.9, with RMSE below 0.5 DU. In contrast, correlation coefficients for tropospheric $O_3$ simulated by WRF-Chem ranged from 0.6 to 0.9, and RMSE values fell between 0.5 and 1.1 DU (see Fig. 2a). For the climatological state (2001–2020): Stratospheric $O_3$ simulated by WRF-Chem showed correlation coefficients exceeding 0.9 and RMSE below 0.5 DU. For tropospheric $O_3$, the model's correlation coefficients ranged from 0.3 to 0.95, with RMSE values between 0.3 and 1.2 DU(see Fig. 3a). Overall, across both La Niña years and the climatological state, WRF-Chem demonstrated superior performance compared to WACCM in simulating tropospheric $O_3$—a finding further supported by the results presented in Fig. 2a and Fig. 3a.

For other key meteorological variables, WRF-Chem outperforms WACCM in simulating zonal wind, geopotential height, and temperature within the 200–500 hPa pressure layer. That said, relatively large simulation errors persist for meridional wind—an observation worth noting when interpreting the model results. Moreover, WRF-Chem demonstrates even greater skill in simulating atmospheric fields at higher altitudes (i.e., above 200 hPa, aligned with the vertical domain defined in this study). Detailed comparisons of these meteorological variable simulations are presented in Supplementary Figs. S1–S12.

Overall, the single-synthetic simulation approach implemented with WRF-Chem can, to a certain extent, serve as a viable substitute for multi-year WACCM simulations. Notably, this approach also offers superior performance in representing key

https://doi.org/10.5194/egusphere-2026-2146
Preprint. Discussion started: 4 May 2026


185 tropospheric meteorological variables—specifically zonal wind, geopotential height, and temperature—consistent with the simulation results discussed earlier.

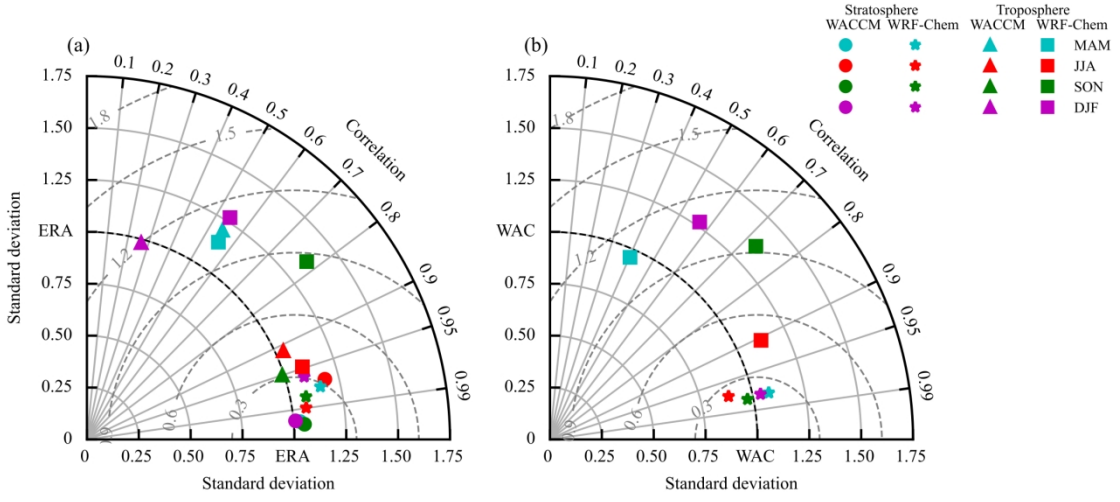


**Figure 1. Taylor diagrams of total column ozone (TCO) in the stratosphere (100–200 hPa) and troposphere (250–500 hPa) during spring (MAM), summer (JJA), autumn (SON), and winter (DJF) of El Niño years. (a) Spatial distribution performance of**
190 **stratospheric and tropospheric TCO compared with ERA5 reanalysis, with different seasons indicated by colors. Symbols denote Stratospheric WACCM (circle), Tropospheric WACCM (triangle), Stratospheric WRF-Chem (pentagram), and Tropospheric WRF-Chem (square). (b) Spatial distribution performance of stratospheric and tropospheric TCO in WRF-Chem compared with WACCM across different seasons, using the same symbol and color scheme.**

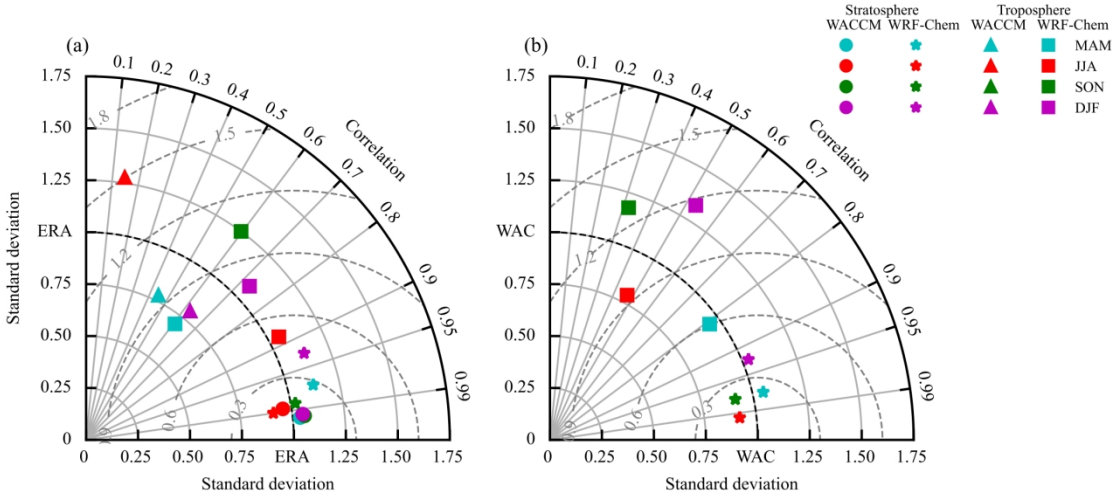


195 **Figure 2. The same as Fig. 1, but for La Niña year.**

https://doi.org/10.5194/egusphere-2026-2146
Preprint. Discussion started: 4 May 2026


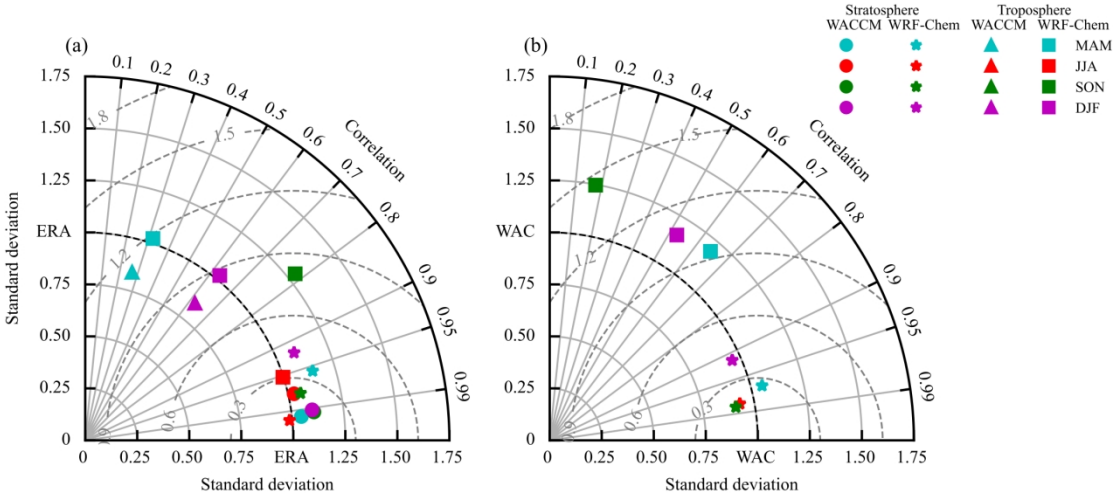


**Figure 3. The same as Fig. 1, but showing the climate states from 2001 to 2020.**

### 2.4 three-dimensional labelling algorithm

To identify the frequency and location of STT events over the TP, the three-dimensional (3D) labelling algorithm put forward by Škerlak et al. (2015) was utilized. The process can be outlined as follows: Using 6 - hourly reanalysis data, an occurrence is categorized as a STT event at a specific location if three distinct atmospheric levels are detected. These levels must meet two conditions simultaneously: the potential vorticity is equal to 2 potential vorticity units (PVU), and the specific humidity is less than 0.1 g $kg^{-1}$. The pressures at the lowest, middle, and highest of these three levels are respectively denoted as $P_{max}$, $P_{me}$, and $P_{min}$. As per the classification approach of Tyrlis et al. (2014), the folding type can be determined by the pressure difference $\Delta p = P_{me} - P_{min}$. However, in this study, no further subclassification of folding types was carried out; instead, only the total count of folding events was subjected to statistical analysis.

### 2.5 Calculation of the BDC

The BDC—a key stratospheric $O_3$ transport process driven by planetary waves—redistributes stratospheric $O_3$ and modifies its spatial distribution. In atmospheric dynamics, residual circulation is widely used to characterize the dynamical behavior of the BDC (Butchart, 2014), as it effectively isolates the slow, large - scale meridional and vertical transport components that dominate $O_3$ redistribution in the stratosphere. To investigate the mechanisms governing stratospheric $O_3$ concentration changes under the influence of the ENSO, this study employed the method proposed by Edmon et al. (1980) for residual circulation calculation. The formula used to compute the residual circulation is as follows:

$$\overline{v}^{*} = \overline{v} - [\overline{(v'\theta')}/\overline{\theta}_p]_p, \quad (1)$$

https://doi.org/10.5194/egusphere-2026-2146
Preprint. Discussion started: 4 May 2026


$$\overline{\omega}^{*} = \overline{\omega} + (a\cos\phi)^{-1}[\cos\phi(\overline{(v^{'}\theta^{'})}/\overline{\theta}_{p})]_{\phi}, \quad (2)$$

Where $\theta$ represents potential temperature; a is the Earth's radius; $\overline{v}$ is the mean meridional wind; and $\overline{\omega}$ is the mean vertical velocity in the pressure coordinate system. The subscripts p and $\phi$ indicate derivatives with respect to pressure (P) and latitude ($\phi$), respectively. $v^{'}$ and $\theta^{'}$ denote the deviations of the meridional wind and potential temperature from their regional averages.

### 2.6 Calculation of the Hadley circulation

The Hadley Circulation (HC) is one of the most prominent large - scale atmospheric circulations in the global climate system. It plays a pivotal role in sustaining the STJ, with the position and intensity of the STJ being closely tied to HC variability (Duan et al., 2023). Notably, the location and strength of the STJ further exert a regulatory influence on the occurrence and frequency of STT events (Albers et al., 2018; Yin et al., 2023). Through this cascading relationship—HC regulating STJ, which in turn modulates STT—different phases of the ENSO alter the strength and location of the HC (Sun, 2018; Li et al., 2024). This HC adjustment, in turn, modulates the intensity and position of the STJ. Ultimately, this chain of effects impacts the spatiotemporal distribution of stratospheric $O_3$ entering the troposphere and, by extension, influences tropospheric $O_3$ concentrations.

HC is typically quantified using the meridional mass streamfunction (MMS) (Qian et al., 2016), and the corresponding equation calculated following Eq. (3):

$$\mathrm{MMS} = \frac{2\pi a\cos\phi}{g}\int_{p_s}^{p} v(p,\phi)\,dp \quad (3)$$

Where $v$ represents the meridional wind; $\phi$ denotes latitude; p is the pressure; $p_s$ is the surface pressure; a is the Earth's radius; and g is the gravitational acceleration.

## 3 Result

### 3.1 TCO impact of ENSO

Consistent with the regulatory relationship between STJ and STT established earlier, STT is strongly influenced by the STJ—with the spatiotemporal distribution of STT primarily controlled by the position and intensity of the STJ (Lamarque and Hess, 1994; Holton et al., 1995; Stohl et al., 2003; Luo et al., 2019). To specifically identify STT events associated with the STJ (and thereby isolate the jet stream-driven component of STT), this study adopted the methodological approach proposed by Olsen et al. (2019) to determine the jet stream axis. On this basis, STT events occurring within a ± 20° latitude

https://doi.org/10.5194/egusphere-2026-2146
Preprint. Discussion started: 4 May 2026


range relative to this axis were selected for further analysis—this latitudinal constraint ensures that the selected events are closely linked to STJ dynamics.

Using the 3D labeling algorithm, this study analyzed the distribution of STT events over the TP during El Niño and La Niña years. The results reveal that STT anomalies exhibit an almost opposite north–south phase between the two ENSO phases, with the frequency of STT events being significantly higher during El Niño years than during La Niña years (see Fig. 4). Consistent with previous findings, these STT anomalies are modulated by STJ anomalies and characterized by meridional displacements (Luo et al., 2019; Yin et al., 2023). Further, the 200 hPa wind field anomalies simulated by WRF-Chem (see Figs. 5e–h, 6e–h, and 7e–h) show that seasonal wind anomalies during El Niño and La Niña years also occur in opposing phases. Specifically:

(1) During El Niño years: The STJ shifts westward and southward in spring, moves southward in summer, extends eastward in autumn, and retreats westward in winter. (2) During La Niña years: The STJ exhibits the opposite seasonal behavior.

This seasonal evolution of the STJ closely corresponds to the positive and negative STT anomalies shown in Fig. 4, indicating that the ENSO exerts a significant influence on the frequency of STT events over the TP.As STT is a key process influencing tropospheric $O_3$ concentrations—with its occurrence location partially determining the spatial distribution of tropospheric $O_3$—the amount of stratospheric $O_3$ entering the troposphere during STT events is further regulated by $O_3$ concentrations in the lower stratosphere. To comprehensively assess STT's impact, this study considered both the anomalous STT patterns during El Niño/La Niña years and the diffusion of stratospheric tracers in the troposphere (noting that Fig. 4 reflects only STT frequency, not intensity). The results show that stratospheric tracer anomalies simulated by WRF-Chem (see Figs. 5i–l and 6i–l) are in good agreement with STT event anomalies (Fig. 4).

Quantitatively, the mean stratospheric tracer flux into the troposphere exhibits the following seasonal differences relative to the climatological state:

**Table 2 The Mean Stratospheric Tracer Flux Relative to the Climatological State**

| ENSO Phase | Spring | Summer | Autumn | Winter |
|---|---|---|---|---|
| El Niño | 760% higher | 13% higher | 0.5% lower | 31% higher |
| La Niña | 120% higher | 50% higher | 44% lower | 3.6% higher |

Note: flux data are not shown in figures. These results indicate that, except in summer, the transport of stratospheric air into the troposphere is generally greater during El Niño years than during La Niña years—suggesting that the TP is more susceptible to STT events under El Niño conditions.

https://doi.org/10.5194/egusphere-2026-2146
Preprint. Discussion started: 4 May 2026


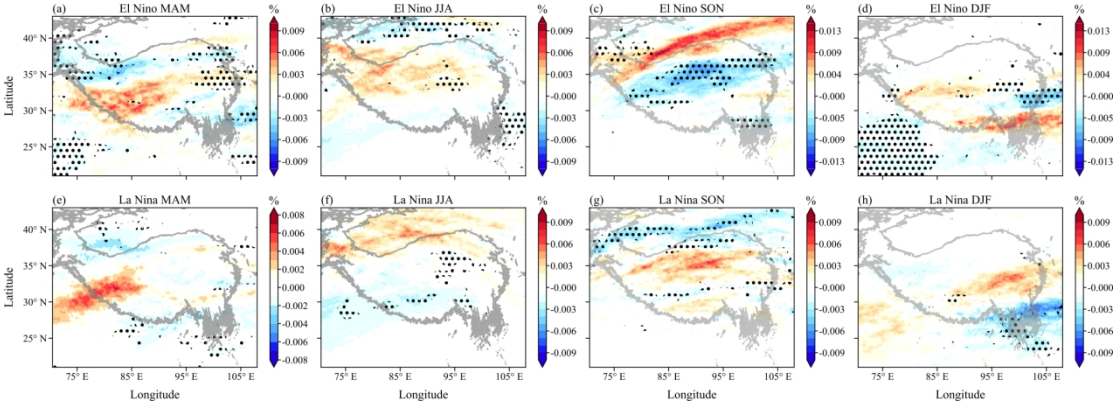


**Figure 4. Seasonal anomaly distributions of STT events in different phases of ENSO. (a-d) the anomalies in MAM, JJA, SON and DJF during El Niño (Unit: %), respectively, and (e-h) the anomalies of La Niña (Unit: %). Black dots denotes statistically significant anomalies at the 95 % confidence level according to the Student's t-test.**

TCO in the lower stratosphere is strongly modulated by the ENSO. The peak magnitudes of these anomalies are documented in Table 3. It indicates enhanced ozone concentrations in the lower stratosphere in El Niño years during spring and summer, potentially exerting stronger downward influence on tropospheric systems compared to La Niña events. A seasonal analysis reveals that during spring, summer, and winter, TCO anomalies in El Niño and La Niña years generally exhibit opposite-phase patterns. In contrast, autumn shows no significant difference in TCO anomalies between the two ENSO phases (see Figs. 5a – d, 6a – d). This seasonal dependence of TCO anomalies may be attributed to two key factors: First, ENSO forcing weakens from late summer onward, which in turn leads to a concurrent attenuation of the associated BDC anomalies — given that BDC dynamics play a critical role in regulating stratospheric ozone distribution. Second, the influence of other dynamical factors (e.g., the QBO) may exceed or counteract ENSO's effect during autumn. Consistent with this hypothesis, previous studies have demonstrated that stratospheric ozone is highly sensitive to both ENSO and QBO: their respective influences on ozone exhibit comparable amplitudes but opposite phases, and the combined effect of ENSO and QBO on ozone can be approximated as the linear superposition of their independent contributions (Olsen et al., 2019; Xie et al., 2020). This further supports the notion that QBO-induced variability may mask ENSO's signal in autumn TCO anomalies over the TP. Consequently, the response of TCO to the ENSO and QBO may either partially cancel out or mutually reinforce one another, depending on the phase alignment of the two oscillations. Beyond ENSO and QBO, Sudden Stratospheric Warming (SSW) events can also modulate lower stratospheric $O_3$: they increase lower stratospheric $O_3$ concentrations and alter the stratosphere-to-troposphere $O_3$ flux, introducing an additional layer of complexity to $O_3$ variability (Tian et al., 2023; Lee et al., 2025). In addition to regulating the BDC, ENSO exerts a significant influence on the geopotential height field over the TP, generating an anomalous east – west reversed pattern (see Figs. 5a – d, 6a – d, 7a – d). Critically, positive (negative) geopotential height anomalies over the TP correspond to negative (positive) TCO anomalies— a key dynamical link through which ENSO affects regional TCO (Li et al., 2024; Yuan et al., 2025). The physical mechanism underlying this relationship is as follows: a decrease (increase) in geopotential height induces a descent (ascent)

https://doi.org/10.5194/egusphere-2026-2146
Preprint. Discussion started: 4 May 2026


of the tropospheric apex, which in turn leads to an increase (decrease) in TCO in the upper troposphere and lower stratosphere (UTLS) region. Notably, significant negative $O_3$ anomalies persist in the central TP (around 35° N) during both El Niño and La Niña years—with the sole exception of summer in El Niño years. This persistence, despite the removal of QBO and SSW signals, suggests that these negative $O_3$ anomalies may stem from systematic biases in the model simulations. The underlying physical mechanisms driving these anomalies remain unclear and require further investigation; ideally, future studies should validate and refine these findings using high-resolution observational datasets tailored to the TP region.

The response of tropospheric $O_3$ over the TP to the ENSO is weaker than that of $O_3$ in the lower stratosphere. The peak magnitudes of these anomalies are documented in Table 4. In El Niño years, peak TCO anomalies in the lower stratosphere exceed those in corresponding seasons of La Niña years, while tropospheric TCO peaks likewise maintain higher magnitudes. This demonstrates that lower stratospheric TCO indeed influences tropospheric TCO via STT events. Specifically, significant ENSO-related signals in tropospheric $O_3$ are spatially confined: they are mainly restricted to regions south of 32° N during winter and spring, and south of 35° N during summer. Within these regions, tropospheric $O_3$ anomalies exhibit opposite-phase distributions between El Niño and La Niña events (see Figs. 5e – h, 6e – h). Notably, a key feature emerges: even in areas where STT shows positive (negative) anomalies, tropospheric $O_3$ anomalies in some subregions still display negative (positive) values. This seemingly contradictory pattern aligns with the corresponding $O_3$ anomalies in the lower stratosphere—suggesting that the $O_3$ content in the lower stratosphere exerts a more dominant control on tropospheric $O_3$ variations associated with STT than the frequency of STT events themselves, further validating the role of lower stratospheric $O_3$ content as a key modulator. To further emphasize the contrasting behavior of tropospheric $O_3$ between El Niño and La Niña events over the TP, this study additionally conducted a comparison of composite $O_3$ anomalies between El Niño and La Niña years. This composite analysis helps isolate the ENSO-driven signal from other sources of variability, providing clearer insights into the differential responses of tropospheric $O_3$ to the two ENSO phases.

Across all seasons, a good correspondence is observed between lower stratospheric TCO anomalies and geopotential height anomalies over the TP (see Fig.7a – d). However, north of 35° N, TCO anomalies during non-summer seasons cannot be fully explained by geopotential height anomalies alone. This residual variability likely reflects the regulatory influence of the BDC, a mechanism that will be further discussed in Sect.3.2. In addition, lower stratospheric TCO anomalies exert an impact on tropospheric TCO distributions through STT processes—this linkage is particularly pronounced in autumn and winter (see Fig.7g, h). By contrast, seasonal discrepancies emerge in spring and summer: In spring:Tropospheric TCO anomalies exhibit an opposite phase relative to both stratospheric TCO anomalies and stratospheric tracer signals. In summer: Tropospheric TCO anomalies also show an opposite phase compared with stratospheric tracer signals (see Fig.7e, f). These contrasting patterns suggest that tropospheric TCO variations in spring and summer are modulated by additional processes beyond STT. For instance, severe springtime and summertime air pollution over the TP is closely tied to South Asian (Yang et al., 2023) and Russia (Zhang et al., 2021) biomass burning, and springtime burning activity itself is sensitive to ENSO variability (Xue et al., 2021)—introducing an ENSO-driven anthropogenic/natural emission pathway for tropospheric $O_3$.

https://doi.org/10.5194/egusphere-2026-2146
Preprint. Discussion started: 4 May 2026


Although summertime burning activity may not be related to ENSO, it is included in the synthetic analysis of El Niño. In summer, under the enhanced South Asian High during La Niña years (see Fig.7b), increased transport of low-concentration surface $O_3$ to the upper troposphere occurs, leading to positive TCO anomalies south of 35° N. This transport mechanism also represents a key contributor to the formation of the summertime $O_3$ valley over the TP (Bian et al., 2011). To gain deeper insight into these season-specific processes, Sect.3.2 will further examine two critical regions: the spring hotspot region (30 – 35° N, 80 – 92° E; red box in Fig.7e) and the summer key region (28 – 33° N, 80 – 92° E; blue box in Fig.7f). TCO over the TP is markedly influenced by ENSO, with indications of a complex feedback between the two. The preceding analysis highlights the important contribution of lower stratospheric $O_3$ to tropospheric $O_3$. Accordingly, the following section focuses on how ENSO modulates lower stratospheric $O_3$ via changes in the stratospheric BDC.

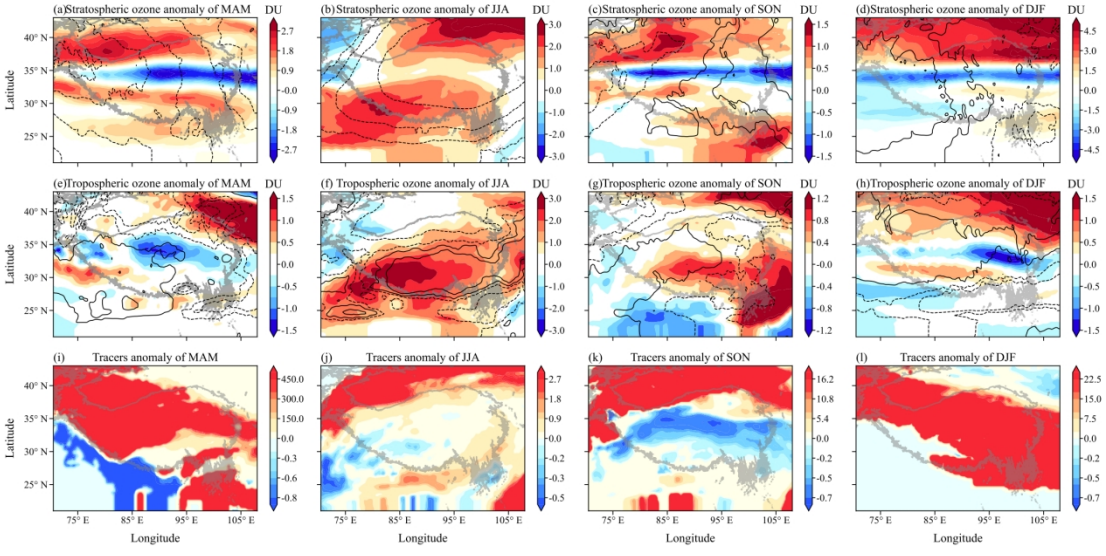


**Figure 5. Anomalies in TCO and stratospheric tracers for MAM, JJA, SON, DJF seasons of El Niño years. (a–d) Stratospheric (100–200 hPa) TCO anomalies (shading; DU). Contours denote 200 hPa geopotential height anomalies (solid: positive, dashed: negative). (e–h) Tropospheric (300–500 hPa) TCO anomalies (shading; DU). Contours denote 200 hPa wind speed anomalies (solid: positive, dashed: negative). (i–l) Ratio of stratospheric tracer anomalies entering the troposphere (300–500 hPa) to the climatological mean (shading). Areas exceeding the color scale maximum (minimum) indicate regions where the climatological mean (El Niño) experiences negligible influence from STT.**

https://doi.org/10.5194/egusphere-2026-2146
Preprint. Discussion started: 4 May 2026


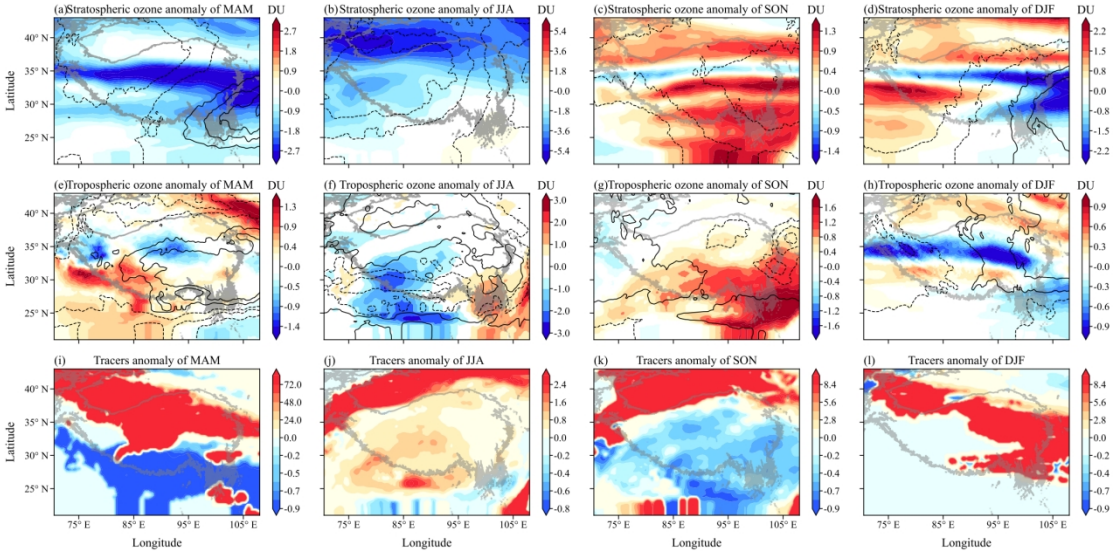


**Figure 6. The same as Fig. 5, but for La Niña year.**

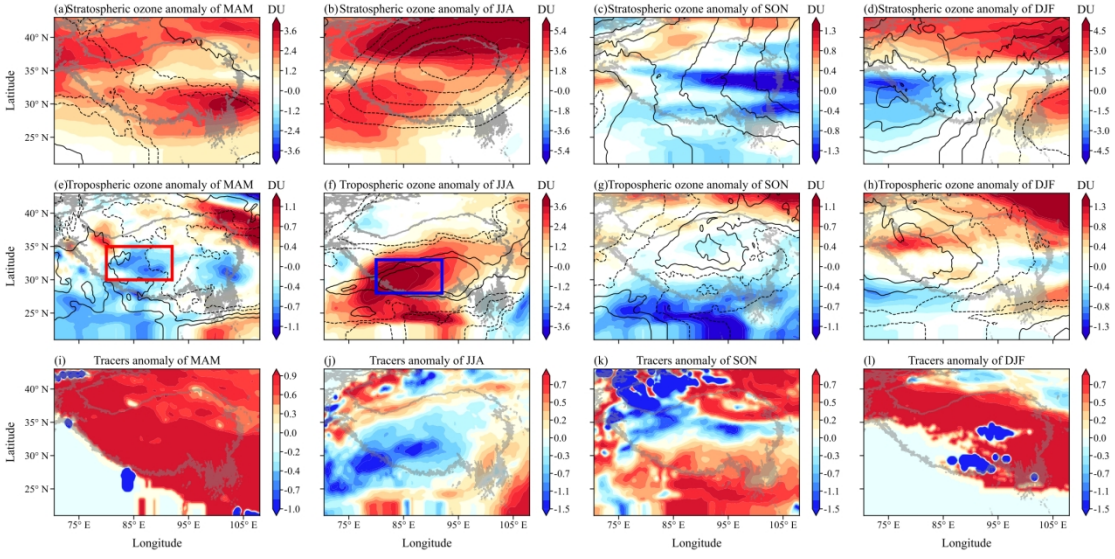


**Figure 7. TCO anomalies during El Niño and La Niña events for MAM, JJA, SON, and DJF seasons. (a–d) Stratospheric (100–200 hPa) TCO anomalies (shading; DU). Contours denote 200 hPa geopotential height anomalies (solid: positive, dashed: negative). (e–h) Tropospheric (300–500 hPa) TCO anomalies (shading; DU). Contours denote 200 hPa wind speed anomalies (solid: positive, dashed: negative). (i–l) Ratio of stratospheric tracer anomalies entering the troposphere (300–500 hPa) to the climatological mean (shading; unitless). Areas exceeding the upper (lower) bound of the color scale indicate regions where La Niña (El Niño) experiences negligible influence from STT compared to El Niño (La Niña).**

https://doi.org/10.5194/egusphere-2026-2146
Preprint. Discussion started: 4 May 2026


**Table 3 The Peak Anomalies of TCO in the Lower Stratosphere under Distinct ENSO Phases**

| ENSO Phase | Spring (DU) | Summer (DU) | Autumn (DU) | Winter (DU) |
|---|---|---|---|---|
| El Niño | 2.79, -3.49 | 4.41, -1.96 | 1.44, -1.71 | 1.66, -4.20 |
| La Niña | 0.30, -4.03 | 1.01, -5.88 | 1.71, -0.83 | 2.55, -4.16 |

Note: as the winter ENSO-induced anomalies exhibit an east-west dipole pattern only south of 35° N, the peak magnitude of winter anomalies is quantitatively assessed solely in this latitudinal belt.

**Table 4 The Peak Anomalies of TCO in the Troposphere under Distinct ENSO Phases**

| ENSO Phase | Spring (DU) | Summer (DU) | Autumn (DU) | Winter (DU) |
|---|---|---|---|---|
| El Niño | 2.70, -1.83 | 3.16, -1.71 | 1.71, -0.93 | 0.95, -1.55 |
| La Niña | 1.98, -1.58 | 2.65, -2.75 | 2.20, -0.55 | 0.60, -1.43 |

Note: as the winter ENSO-induced anomalies exhibit an east-west dipole pattern only south of 35° N, the peak magnitude of winter anomalies is quantitatively assessed solely in this latitudinal belt.

### 3.2 Driving mechanisms of $O_3$ anomalies

Following the peak of the El Niño event, the deep branch of the BDC above the TP weakens. This weakening leads to two key effects: (1) negative $O_3$ anomalies in the upper stratosphere north of 35° N; and (2) reduced downward transport of upper stratospheric $O_3$, which in turn induces negative $O_3$ anomalies in the lower stratosphere near 35° N. From April onward, the deep branch of the BDC strengthens slightly but remains weaker than its climatological state. During this period, the negative $O_3$ anomalies in the lower stratosphere around 35° N are largely attributed to the persistence of anomalies established in March, rather than direct downward transport from the upper stratosphere. In May and June, positive $O_3$ anomalies emerge in the upper stratosphere; however, the persistently weak deep branch inhibits the downward transport of these positive anomalies, preventing them from propagating to the lower stratosphere. In May, the positive $O_3$ anomalies in the lower stratosphere north of 35° N are influenced by the upper stratosphere, while the $O_3$ anomalies in June are the residuals of May's anomalies, not directly affected by the upper stratosphere. Concurrently, the shallow branch of the BDC intensifies in May, transporting tropospheric air with low $O_3$ concentrations upward into the lower stratosphere—this upward transport generates weak negative $O_3$ anomalies in the lower stratosphere. From July to November, negative $O_3$ anomalies recur in the upper stratosphere north of ~35° N. Prior to October, the corresponding negative $O_3$ anomalies in the lower stratosphere are primarily driven by the enhanced or weakened shallow branch and the persistence of anomalies established in the preceding month. After October, the combined effect of a further weakened deep branch and a strengthened shallow branch reinforces the negative $O_3$ anomalies in the lower stratosphere near ~35° N. At this stage, $O_3$ in the lower stratosphere is influenced by the joint effects of both upper stratospheric and upper tropospheric $O_3$. By December, the deep branch of the BDC intensifies abruptly, triggering widespread positive $O_3$ anomalies in the upper stratosphere—a pattern that persists

https://doi.org/10.5194/egusphere-2026-2146
Preprint. Discussion started: 4 May 2026


throughout winter. These enhanced upper stratospheric $O_3$ concentrations are efficiently transported downward and affect the lower stratosphere. But in February, despite the weakening of the shallow branch of the BDC, the lower stratospheric $O_3$ forms negative anomalies due to the sudden emergence of negative $O_3$ anomalies in the middle stratosphere (see Fig. 8).

In La Niña years, the phase characteristics of the BDC are largely opposite to those observed during El Niño years. However, stratospheric $O_3$ anomalies do not exhibit a strictly opposite-phase response across all seasons and regions (see Fig. 9)—a finding that suggests the ENSO is not the sole driver of stratospheric $O_3$ variability (Tian et al., 2023; Zhang et al., 2025). In March, negative $O_3$ anomalies persist in the upper stratosphere north of ~35° N and extend continuously through November. During this period, the concurrent negative $O_3$ anomalies in the lower stratosphere at the same latitude (north of ~35° N) reflect the combined regulatory influence of both the deep and shallow branches of the BDC. In April, negative $O_3$ anomalies in the lower stratosphere emerge under the influence of negative $O_3$ anomalies in the upper stratosphere and the enhanced shallow branch. In May, the lower stratosphere is primarily influenced by the negative $O_3$ anomalies in the upper stratosphere. From June to September, the deep branch of the BDC remains neutral, showing no significant weakening, but negative $O_3$ anomalies persist in the upper stratosphere. In June and July, the negative $O_3$ anomalies in the lower stratosphere are mainly the residuals of May's negative anomalies, with minimal influence from the upper stratosphere. In August, the positive $O_3$ anomalies in the middle and upper stratosphere, along with the weakened shallow branch, jointly affect the lower stratospheric $O_3$, causing it to exhibit positive anomalies. In September, the shallow branch strengthens, but the lower stratosphere's $O_3$ is primarily influenced by the residual positive $O_3$ anomalies from the middle stratosphere in August. After October, the deep branch strengthens, and although the shallow branch continues to influence lower stratospheric $O_3$ concentrations, the $O_3$ anomalies in the upper stratosphere play a dominant role in influencing the lower stratosphere.

In conclusion, the ENSO exerts a pronounced regulatory influence on lower stratospheric $O_3$ over the TP. From a seasonal perspective, the BDC—a key mediator of this ENSO-$O_3$ linkage—exhibits distinct branch-dominant patterns: from late autumn to early spring, lower stratospheric $O_3$ is modulated by both the deep and shallow branches of the BDC, with the deep branch playing the dominant role; whereas during other periods, it is primarily dominated by the shallow branch of the BDC. Overall, the BDC weakens during El Niño years and strengthens during La Niña years—a phase-dependent response that directly modulates $O_3$ transport efficiency in the stratosphere. This BDC-mediated mechanism accounts for the marked seasonal discrepancies between stratospheric $O_3$ anomalies and geopotential height anomalies north of 35° N, with the exception of summer (see Fig. 7a – d). These findings collectively reflect the strong control of BDC transport processes on stratospheric $O_3$ variability over the TP, highlighting the critical role of the BDC in bridging ENSO forcing and regional $O_3$ responses.

To further unravel the mechanisms underlying the differences between tropospheric and lower stratospheric $O_3$ anomalies over the TP, detailed follow-up analyses will be conducted targeting two key regions: the red-framed region in Fig. 7e (spring focus: 30–35° N, 80–92° E) and the blue-framed region in Fig. 7f (summer focus: 28–33° N, 80–92° E). These targeted analyses will systematically examine the regulatory roles of three critical atmospheric factors: the temperature field,

https://doi.org/10.5194/egusphere-2026-2146
Preprint. Discussion started: 4 May 2026


vertical circulation, and geopotential height field. By quantifying the contributions of each factor to $O_3$ variability across the troposphere and lower stratosphere, the analyses aim to clarify why $O_3$ anomaly patterns differ between these two atmospheric layers—addressing the unresolved questions raised by the seasonal discrepancies observed in previous results.

The $O_3$ anomalies over the central TP are strongly regulated by local thermodynamic and dynamic processes. Specifically, surface cooling (or heating) induces anomalous descending (or ascending) air currents, which are accompanied by corresponding decreases (or increases) in geopotential height. Anomalous descending motion facilitates the downward transport of stratospheric $O_3$—sourced from regions with low potential height—into the troposphere, thereby leading to positive tropospheric $O_3$ anomalies. Conversely, anomalous ascending motion transports $O_3$-poor air from the lower troposphere to the upper troposphere, resulting in negative tropospheric $O_3$ anomalies. This regulatory pattern is clearly evident during specific periods, such as 10–29 May and 26 March–1 April (see Fig. 10). It should be noted, however, that not all STT events exert a strong influence on near-surface $O_3$. For instance, in Fig. 10a, the negative tropospheric potential vorticity (PV) anomaly does not extend below 400 hPa—indicating limited downward penetration of stratospheric signals—yet substantial negative $O_3$ anomalies (with magnitudes up to 42.8 ppbv) are still observed in the troposphere. Given that vertical transport over this region is predominantly downward in spring, the contribution of upward transport of $O_3$-poor air from the lower troposphere to these negative anomalies can be ruled out. Furthermore, a temporal discrepancy emerges: following 7 March, 11 April, 6 May, and 16 May, negative tropospheric $O_3$ anomalies appeared earlier than the corresponding negative PV anomalies at the tropopause (a key indicator of STT activity). Together, these two lines of evidence—the limited vertical penetration of PV anomalies and the temporal asynchrony between $O_3$ and PV anomalies—suggest that negative tropospheric $O_3$ anomalies over the central TP are not solely controlled by STT processes. Additional factors, including biomass burning emissions and regional horizontal transport, may also play important regulatory roles in shaping these $O_3$ anomalies.

In summer, the thermal forcing of the TP intensifies—this enhancement increases the region's sensitivity to ENSO variability, thereby driving pronounced adjustments in both the geopotential height field and the vertical circulation structure (see Fig. 11). Within the target area (28–33° N, 80–92° E), a prevailing downward motion characterizes the vertical circulation during both El Niño and La Niña years, though distinct ENSO-phase differences emerge in the strength of this motion and associated atmospheric anomalies. During La Niña summers, anomalous tropospheric warming weakens the downdraft and elevates the geopotential height; this elevation of geopotential height further causes the dynamical tropopause to rise, which in turn suppresses the effective downward transport of stratospheric air into the troposphere. In contrast, during El Niño summers, substantial positive $O_3$ anomalies develop in the troposphere, with magnitudes reaching up to 38.7 ppbv between 1 June and 2 August. Notably, the negative tropospheric temperature anomalies associated with El Niño onset as early as May and persist through most of the summer—this early and prolonged cooling likely contributes to the maintenance of favorable conditions for positive $O_3$ anomalies.

In summary, the TP exerts a strong regulatory effect on local dynamical processes through its topographic thermal forcing. This thermal-driven modulation of dynamics further influences tropospheric $O_3$ anomalies via dynamical feedback

https://doi.org/10.5194/egusphere-2026-2146
Preprint. Discussion started: 4 May 2026


mechanisms—creating a clear "topographic thermal forcing → dynamical process adjustment → tropospheric $O_3$ response" linkage. This regulatory mechanism is particularly prominent in summer: during this season, the ENSO plays a critical role in modulating the TP's thermal state, thereby amplifying or modifying the plateau's influence on local dynamical processes and, in turn, on tropospheric $O_3$ anomalies. This underscores ENSO's role as a key external driver that interacts with the TP's intrinsic thermal forcing to shape regional $O_3$ variability.

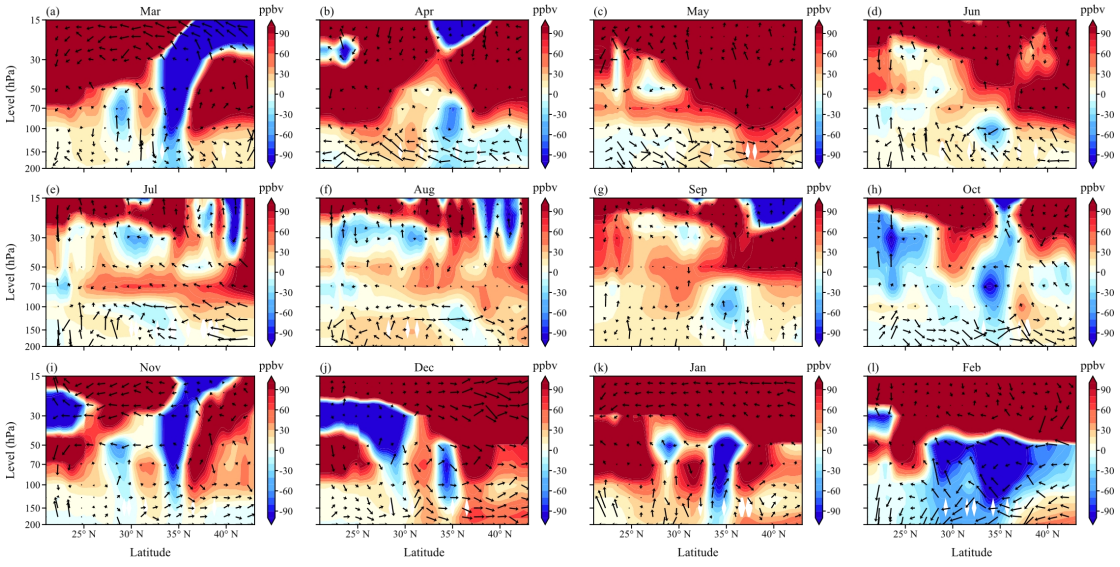


**Figure 8. Anomalies in stratospheric $O_3$ (shading; ppbv) and residual circulation (Vector, $\overline{\omega}^*$ magnified 500; mm $s^{-1}$) during El Niño years.**

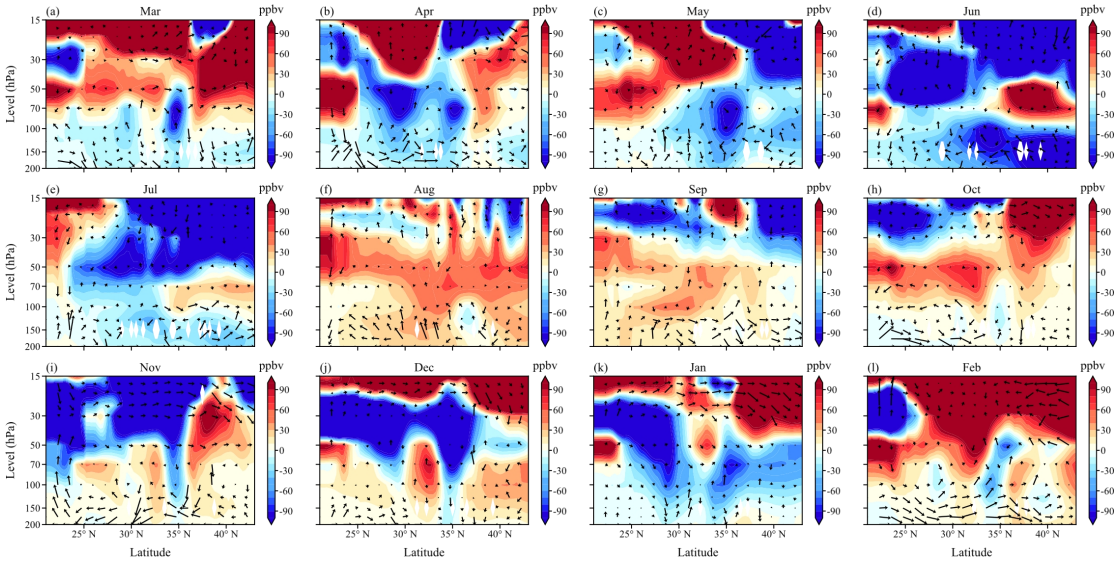


**Figure 9. The same as Fig. 8, but for La Niña years.**

https://doi.org/10.5194/egusphere-2026-2146
Preprint. Discussion started: 4 May 2026


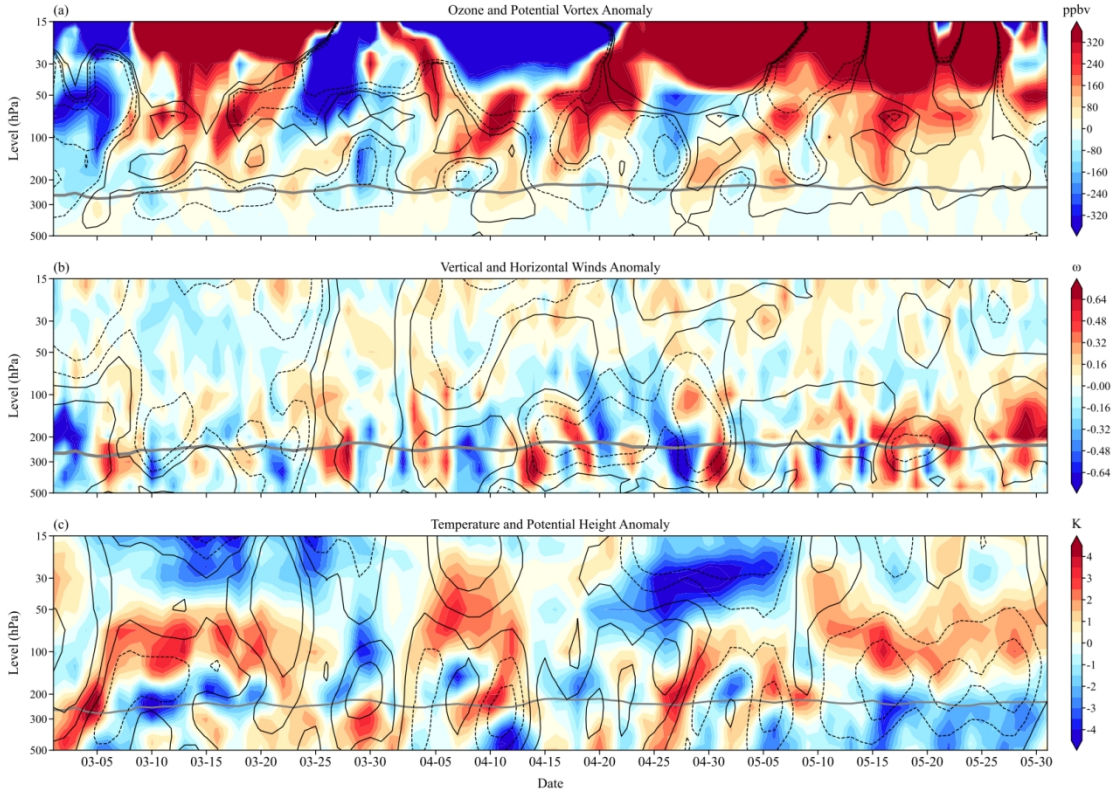


**Figure 10. Anomalies in $O_3$, potential vorticity, residual circulation, vertical velocity, horizontal velocity, temperature, and geopotential height during El Niño and La Niña events at 30° N–35° N and 80° E–92° E in spring. The thick grey solid line denotes the dynamical tropopause (2 PVU). (a) $O_3$ anomalies (shading; ppbv) and potential vorticity anomalies (contours; PVU). (b) Residual circulation anomalies (shading; normalized) above the dynamical tropopause and vertical velocity anomalies (shading; normalized) below it. Contours denote horizontal velocity anomalies (m $s^{-1}$). (c) Temperature anomalies (shading; K) and geopotential height anomalies (contours; gpm).**

https://doi.org/10.5194/egusphere-2026-2146
Preprint. Discussion started: 4 May 2026


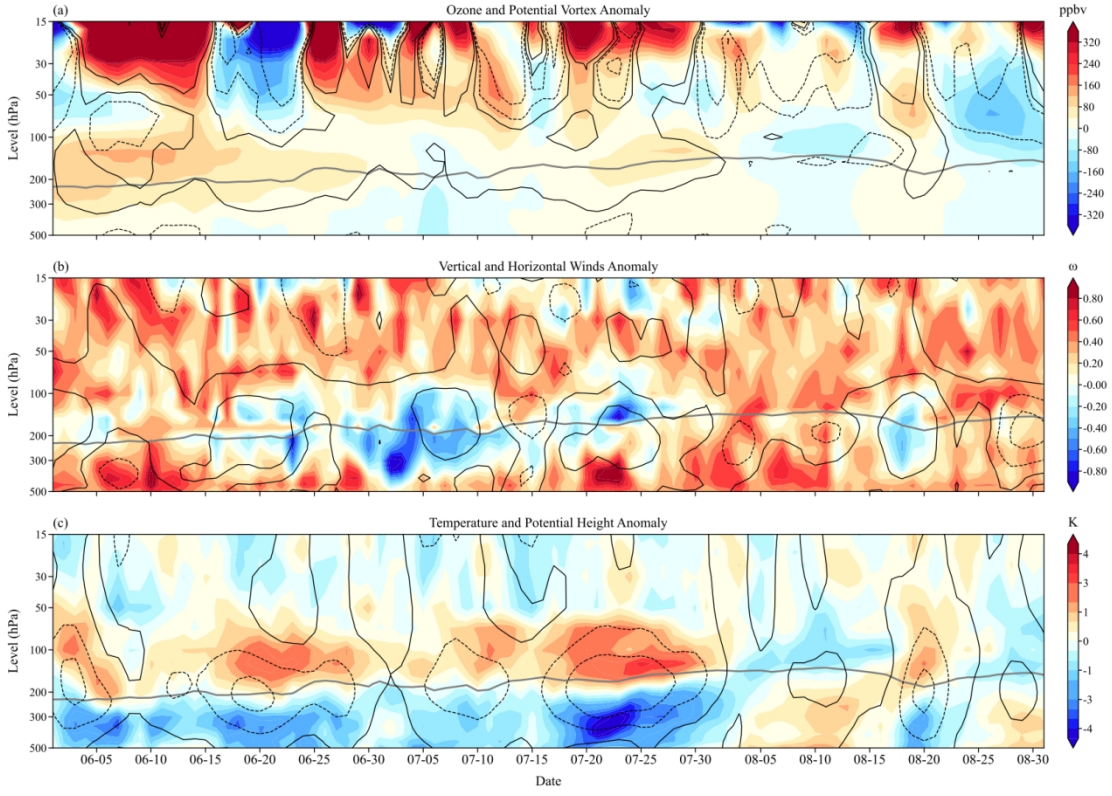


**Figure 11. The same as Fig. 10, but at 28° N–33° N and 80° E–92° E in summer.**

### 3.3 ENSO impact on the STJ over the TP

The position and intensity of the STJ are key factors regulating the location and frequency of STT events—and by extension, they exert a notable influence on the spatial distribution of tropospheric $O_3$. As discussed in Sect. 3.1, STT anomalies during El Niño and La Niña years are significantly modulated by STJ anomalies at the 200 hPa level. Specifically, the spatial distribution of STT anomalies exhibits clear variability that aligns with the seasonal meridional or zonal displacement of the STJ—reflecting a tight dynamical linkage between the jet stream's seasonal movement and STT's spatial pattern. To further elucidate this STJ-STT-$O_3$ linkage and address the mechanisms driving STT differences across ENSO phases, this study analyzed the underlying causes of discrepancies in the 200 hPa STJ (e.g., in position, intensity, or seasonal evolution) between El Niño and La Niña years. This analysis aims to clarify how ENSO-induced STJ anomalies ultimately shape STT's spatial-temporal characteristics and, consequently, tropospheric $O_3$ distribution.

Compared with El Niño years, the STJ exhibits a more northerly displaced position across all seasons during La Niña years (see Fig. 12). Based on the thermal wind balance theory, this inter-ENSO-phase difference in STJ position can largely be attributed to the contrasting thermal anomalies over the TP. During El Niño years, negative temperature anomalies prevail above the TP in spring and summer. This thermal pattern exerts two key effects on meridional temperature gradients: (1) it

https://doi.org/10.5194/egusphere-2026-2146
Preprint. Discussion started: 4 May 2026


enhances the equator–TP meridional temperature gradient; and (2) it reduces the TP–polar meridional temperature gradient. Together, these gradient adjustments drive a southward shift of the STJ, accompanied by the emergence of a positive STJ anomaly south of the TP. In contrast, La Niña years are characterized by positive temperature anomalies above the TP—an opposite thermal signature to that of El Niño years. These positive anomalies weaken the equator–TP meridional temperature gradient while strengthening the TP–polar meridional temperature gradient. Consequently, the STJ shifts northward relative to its El Niño-year position, with a positive STJ anomaly forming north of the TP instead.

For the STJ anomalies in autumn and winter during El Niño years, their partial similarity to some STJ anomalies in La Niña years cannot be fully explained by the thermal wind balance theory alone. An analysis of local HC anomalies reveals that the HC plays a key regulatory role in mediating these STJ patterns—serving as a critical complementary mechanism to the TP-related thermal forcing. In autumn, the HC exhibits a marked southward shift during El Niño years relative to La Niña years. This southward displacement of the HC effectively counteracts the northward shift of the STJ that is induced by the positive temperature anomaly over the TP in El Niño autumns. Conversely, during La Niña autumns, the northward-displaced HC reinforces the northward shift of the STJ driven by TP thermal anomalies, further amplifying the inter-ENSO-phase difference in STJ position. In winter, the HC exhibits contrasting intensity variations across ENSO phases: its intensity weakens during El Niño years but strengthens during La Niña years. This intensity difference partly offsets the influence of TP-related temperature anomalies on the STJ: specifically, the weakened HC in El Niño winters reduces the extent of the STJ's northward shift (which would otherwise be driven by the positive TP temperature anomaly); meanwhile, the enhanced HC in La Niña winters counteracts the southward displacement of the STJ that would result from the negative TP temperature anomaly in La Niña winters. In addition, during summer and autumn, the HC in La Niña years is generally located further north than in El Niño years—a spatial feature that reinforces the northward displacement of the STJ. It is worth noting that although the HC in El Niño springs also shifts slightly northward, the STJ in La Niña springs remains primarily controlled by the positive TP temperature anomaly. This dominant TP thermal signal compensates for the HC phase difference between the two ENSO phases, resulting in the STJ remaining slightly further north in La Niña springs than in El Niño springs.

The unique topographic features of the TP—particularly its pronounced thermal effect—play a crucial regulatory role in modulating STT and its associated atmospheric processes over this region. Our analysis further indicates that, over the TP, the plateau's thermal effect exerts a stronger influence on the STJ than the local HC. This dominant thermal control on the STJ, in turn, governs the location and frequency of STT events—underscoring the TP's thermal effect as a key driver of regional STT variability. Moreover, the thermal state of the TP is closely regulated by ENSO variability (Nie and Li, 2022; Yong et al., 2023). This linkage implies that ENSO can indirectly modulate STT processes over the TP by altering the plateau's thermal conditions: ENSO-induced changes in the TP's thermal state first adjust the STJ's position and intensity, which then further shape the spatiotemporal characteristics of STT events.

https://doi.org/10.5194/egusphere-2026-2146
Preprint. Discussion started: 4 May 2026


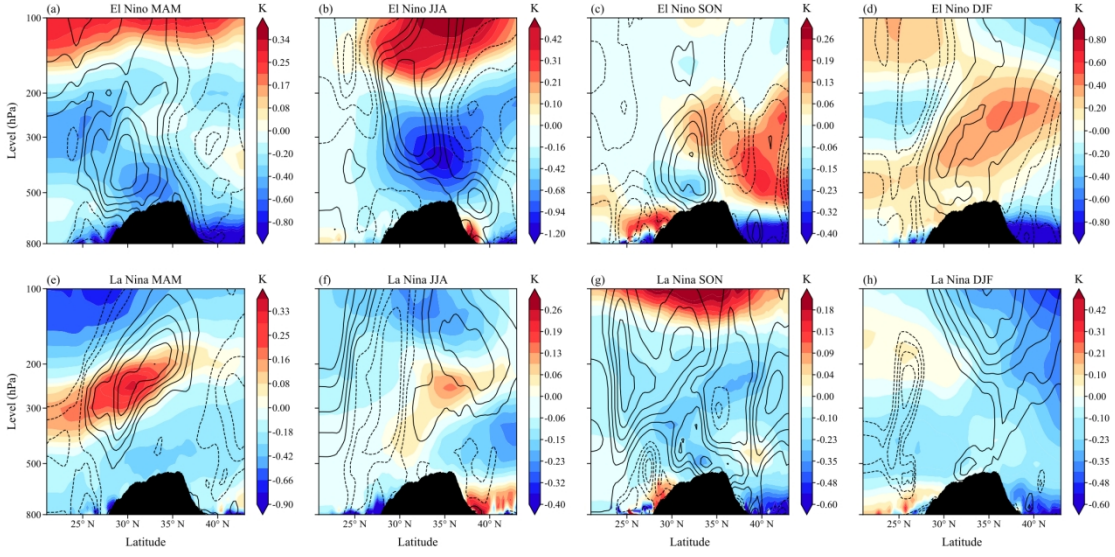


515 **Figure 12. Anomalies in horizontal wind speed and temperature during each season of El Niño and La Niña events. (a–d) Temperature anomalies (shading; K) and horizontal wind speed anomalies (contours; m s⁻¹) for MAM, JJA, SON, and DJF in El Niño years, respectively. (e–h) Temperature anomalies (shading; K) and horizontal wind speed anomalies (contours; m s⁻¹) for MAM, JJA, SON, and DJF in La Niña years, respectively. Black contours denote terrain elevation.**

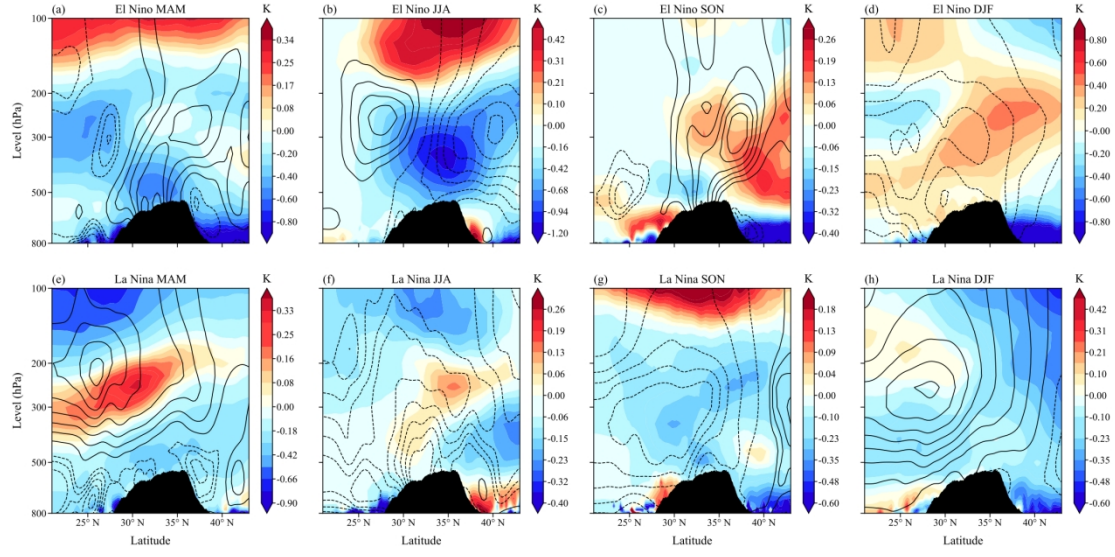


520 **Figure 13. Anomalies in MMS and temperature during each season of El Niño and La Niña events. (a–d) Temperature anomalies (shading; K) and MMS anomalies (contours; 10-8 m s⁻¹) for MAM, JJA, SON, and DJF in El Niño years, respectively. (e–h) Temperature anomalies (shading; K) and MMS anomalies (contours; 10-8 m s⁻¹) for MAM, JJA, SON, and DJF in La Niña years, respectively. Black contours denote terrain elevation.**

https://doi.org/10.5194/egusphere-2026-2146
Preprint. Discussion started: 4 May 2026


## 4 Conclusions

Based on WRF-Chem simulations and synthetic experiments conducted over the 2001–2020 period, this study systematically investigated the impacts of ENSO events on TCO over the TP, as well as the underlying physical mechanisms driving these impacts. Model evaluation results indicate that WRF-Chem effectively captures the seasonal variations of lower stratospheric TCO under El Niño, La Niña, and climatological states. In contrast, the model's simulation accuracy for tropospheric TCO is slightly lower than that for stratospheric TCO—reflecting the greater complexity of tropospheric $O_3$ processes (e.g., emissions, chemical reactions, and boundary layer transport) compared to stratospheric $O_3$ dynamics. When compared to WACCM, WRF-Chem exhibits superior performance in reproducing both tropospheric TCO and key meteorological fields (including zonal wind, geopotential height, and temperature). This advantage is particularly pronounced during El Niño springs and winters—periods characterized by strong ENSO-induced anomalies over the TP. These results collectively highlight WRF-Chem's suitability for conducting multi-year ENSO-related studies on TCO and associated atmospheric processes over the TP.

The ENSO significantly modulates TCO in the lower stratosphere through the combined effects of TP geopotential height anomalies (Li et al., 2024; Yuan et al., 2025) and BDC variability. During El Niño years, lower stratospheric TCO is generally higher than that in La Niña years during spring and summer, a pattern associated with negative correlations between TCO and TP geopotential height anomalies. In winter, lower stratospheric TCO anomalies exhibit spatial heterogeneity, while autumn TCO is largely decoupled from ENSO variability—this decoupling is likely driven by other atmospheric processes such as the QBO or SSW events (Xie et al., 2020; Lee et al., 2025). Moreover, the BDC changes further control lower stratospheric $O_3$. Specifically, from late autumn to early spring, lower stratospheric $O_3$ is modulated by both the deep and shallow branches of the BDC, with the deep branch playing the dominant role; whereas during other periods, it is primarily dominated by the shallow branch of the BDC. El Niño events weaken the BDC deep branch and modulate the shallow branch in a seasonal manner, thereby shaping the timing and persistence of lower stratospheric $O_3$ anomalies; conversely, La Niña years exhibit nearly opposite BDC patterns (e.g., strengthened deep branch and contrasting seasonal adjustments of the shallow branch). These results collectively highlight that ENSO-driven TP dynamical anomalies (e.g., geopotential height variations) and BDC variability jointly determine the seasonal and spatial patterns of lower stratospheric $O_3$ over the TP region.

Our analysis reveals that the ENSO strongly modulates STT over the TP by driving displacements of the STJ: specifically, El Niño years are characterized by southward STJ displacements, while La Niña years exhibit northward STJ displacements, accompanied by nearly opposite north‐south phase patterns of STT anomalies. Except for autumn in El Niño years, positive STT anomalies generally occur farther south in El Niño years than in La Niña years—this spatial pattern confirms the regulatory role of the STJ in shaping STT frequency, which is consistent with previous findings (Luo et al., 2019; Yin et al., 2023). While STT anomalies directly impact tropospheric $O_3$, tropospheric TCO exhibits inverse-phase characteristics relative to STT anomalies only in specific regions and seasons (e.g., south of 32° N in winter and spring, and south of 35° N

https://doi.org/10.5194/egusphere-2026-2146
Preprint. Discussion started: 4 May 2026


in summer). In contrast, autumn tropospheric TCO is largely controlled by lower stratospheric $O_3$, with weak linkage to STT variability. Interestingly, a notable decoupling emerges: positive (negative) STT anomalies sometimes correspond to negative (positive) tropospheric $O_3$ anomalies. This phenomenon highlights that lower stratospheric $O_3$ content exerts a more dominant influence than STT frequency in shaping tropospheric $O_3$ variability. Seasonal deviations in tropospheric $O_3$ that cannot be explained by STT processes are largely driven by additional atmospheric and emission-related mechanisms. In spring, South Asian biomass burning and regional transport processes enhance tropospheric $O_3$ over the TP, and this enhancement is consistent with ENSO-modulated emission patterns (Xue et al., 2021). In summer, La Niña-induced thermal anomalies over the TP weaken local downdrafts and elevate geopotential height, which in turn suppresses the downward transport of stratospheric $O_3$; by contrast, El Niño years lack this suppression, leading to the formation of positive tropospheric $O_3$ anomalies. These results collectively demonstrate that ENSO governs the spatial and seasonal variability of tropospheric $O_3$ over the TP through three intertwined pathways: STJ-induced shifts in STT, the thermal effect of the TP, and ENSO-modulated emission processes.

The thermal effects of the TP not only modulate the geopotential height field and vertical circulation above the region, but also play a key role in regulating the latitudinal position of the STJ. During the spring and summer of El Niño years, negative temperature anomalies prevail above the TP; according to the thermal wind principle, these anomalies drive the STJ southward relative to its climatological position. Conversely, La Niña years exhibit the opposite thermal and dynamical characteristics: positive TP temperature anomalies induce a northward shift of the STJ relative to the climate state. This finding aligns with the conclusions of Ji et al. (2016) and Bharati et al. (2025) but contrasts with the observations reported by Albers et al. (2018), highlighting the regional specificity of TP thermal forcing in modulating large-scale circulation. We therefore propose that the regional phase differences in the STJ (i.e., disparities in its latitudinal position across different ENSO phases and seasons) are closely tied to the local thermal conditions over the TP. Furthermore, the phase of the STJ (in terms of its meridional displacement) is jointly modulated by the intensity of the HC, which exerts a compensating effect on the thermal-driven STJ shifts. In El Niño springs, the HC shifts significantly northward compared to La Niña years—this northward displacement of the HC partially offsets the southward pull of the STJ induced by TP negative temperature anomalies, ultimately resulting in STJ positions that are relatively similar to those in La Niña years. A analogous compensating effect emerges in autumn and winter: during these seasons, positive TP temperature anomalies in El Niño years would inherently favor a northward STJ shift, but concurrent HC anomalies (e.g., weakened intensity or southward displacement) mitigate this thermal-driven tendency. As a result, the meridional displacement of the STJ between El Niño and La Niña years becomes minimal during autumn and winter, with little apparent difference in their latitudinal positions.

In summary, the unique topographic features of the TP, acting through its pronounced thermal effects, interact with the BDC and the HC to jointly modulate three key atmospheric components: the latitudinal position of the STJ, the distribution of lower stratospheric TCO, and the structure of vertical circulation. This integrated regulatory mechanism—linking TP topography, thermal forcing, and large-scale circulation systems—exerts a profound influence on the spatiotemporal variability of tropospheric TCO over the TP, underpinned by the cascading effects of circulation adjustments on STT and $O_3$

https://doi.org/10.5194/egusphere-2026-2146
Preprint. Discussion started: 4 May 2026


exchange across atmospheric layers. This study has a notable limitation: the chemical initial fields of the WRF-Chem model restrict the scope of analysis to ENSO events occurring on or after 2001, precluding investigations of earlier ENSO cycles. To address this gap and enhance the robustness of conclusions regarding long-term ENSO-TCO relationships over the TP, future work should extend the simulation dataset to incorporate ENSO events prior to 2001. Additionally, integrating multi-source observational data (e.g., satellite retrievals and in-situ measurements) into model validation could further refine the understanding of regional $O_3$ dynamics under ENSO forcing.

## Data availability

The ERA5 dataset is available at https://cds.climate.copernicus.eu/datasets/reanalysis-era5-pressure-levels?tab=overview (last access: December 2023; Copernicus Climate Change Service and Climate Data Store, 2023). The output from the WACCM simulations is available at https://rda.ucar.edu/dssearch/?words=WACCM (last access: June 2025; Gasperini, 2019). The Niño-3.4 SST anomaly index is available at https://psl.noaa.gov/data/correlation/nina34.anom.data (last access: September 2023). The chemical and meteorological boundary conditions for WRF-Chem are obtained from https://www.acom.ucar.edu/cam-chem/cam-chem.shtml (last access: February 2024; Buchholz et al., 2019). The Indian Ocean SST data is available at https://www.metoffice.gov.uk/hadobs/hadisst/data/download.html (last access: October 2023; Met Office Hadley Centre, 2016).

## Author contributions

WHY designed the study. YK and BJC synthesized the initial field of the model. LD conducted the WRF-Chem model experiments. XFH created the figures and wrote the manuscript. LQY provided comments and edited the manuscript.

## Competing interests

The contact author has declared that none of the authors has any competing interests.

## Acknowledgements

We thank for the technical support of the National Large Scientific and Technological Infrastructure “Earth System Numerical Simulation Facility” (https://cstr.cn/31134.02.EL). We are thankful to Cai Lei for their very constructive comments.

https://doi.org/10.5194/egusphere-2026-2146
Preprint. Discussion started: 4 May 2026


**Financial support**

This work was supported by the National Natural Science Foundation of China (Grant No. 42365007), the Second Tibetan Plateau Scientific Expedition and Research Program (STEP) (Grant No. 2019QZKK0604), and the Opening Project of Shanghai Key Laboratory of Atmospheric Particle Pollution and Prevention (LAP3) (Grant No. FDLAP24003).

**References**

Akritidis, D., Katragkou, E., Zanis, P., Pytharoulis, I., Melas, D., Flemming, J., Inness, A., Clark, H., Plu, M., and Eskes, H., 2018: A deep stratosphere-to-troposphere ozone transport event over Europe simulated in CAMS global and regional forecast systems: analysis and evaluation, Atmos. Chem. Phys., 18, 15515-15534, https://doi.org/10.5194/acp-18-15515-2018.

Albers, J. R., Butler, A. H., Langford, A. O., Elsbury, D., and Breeden, M. L., 2022: Dynamics of ENSO-driven stratosphere-to-troposphere transport of ozone over North America, Atmos. Chem. Phys., 22, 13035-13048, https://doi.org/10.5194/acp-22-13035-2022.

Albers, J. R., Perlwitz, J., Butler, A. H., Birner, T., Kiladis, G. N., Lawrence, Z. D., Manney, G. L., Langford, A. O., and Dias, J., 2018: Mechanisms Governing Interannual Variability of Stratosphere-to-Troposphere Ozone Transport, J. Geophys. Res. - Atmos., 123, 234-260, https://doi.org/10.1002/2017jd026890.

Bharati, P., Deb, P., Hunt, K. M. R., Orr, A., Dash, M. K., 2025: ENSO-induced Latitudinal Variation of the Subtropical Jet Modulates Extreme Winter Precipitation over the Western Himalaya. Adv. Atmos. Sci. 42, 427–437. https://doi.org/10.1007/s00376-024-4057-2.

Bian, J., Yan, R., Chen, H., Lu, D., and Massie, S. T., 2011: Formation of the Summertime Ozone Valley over the Tibetan Plateau: The Asian Summer Monsoon and Air Column Variations, Adv. Atmos. Sci., 28, 1318-1325, https://doi.org/10.1007/s00376-011-0174-9.

Bracci, A., Cristofanelli, P., Sprenger, M., Bonafe, U., Calzolari, F., Duchi, R., Laj, P., Marinoni, A., Roccato, F., Vuillermoz, E., and Bonasoni, P., 2012: Transport of Stratospheric Air Masses to the Nepal Climate Observatory-Pyramid (Himalaya; 5079 m MSL): A Synoptic-Scale Investigation, J. Appl. Meteorol. Clim., 51, 1489-1507, https://doi.org/10.1175/jamc-d-11-0154.1.

Bruckner, M., Pierce, R. B., and Lenzen, A., 2024: Examining ENSO-related variability in tropical tropospheric ozone in the RAQMS-Aura chemical reanalysis, Atmos. Chem. Phys., 24, 10921-10945, https://doi.org/10.5194/acp-24-10921-2024.

Buchholz, R. R., Emmons, L. K., Tilmes, S., and The CESM2 Development Team, 2019: CESM2.1/CAM-chem Instantaneous Output for Boundary Conditions, UCAR/NCAR - Atmospheric Chemistry Observations and Modeling Laboratory [data set], https://doi.org/10.5065/NMP7-EP60.

Butchart, N., 2014: The Brewer-Dobson circulation, Rev. Geophys., 52, 157-184, https://doi.org/10.1002/2013rg000448.

Chen, H., Xu, C. Y., and Guo, S., 2012: Comparison and evaluation of multiple GCMs, statistical downscaling and hydrological models in the study of climate change impacts on runoff, J. Hydrol., 434, 36-45, https://doi.org/10.1016/j.jhydrol.2012.02.040.

Chen, W. H., Wang, W. W., Jia, S. G., Mao, J. Y., Yan, F. H., Zheng, L. M., Wu, Y. K., Zhang, X. T., Dong, Y. T., Kong, L. B., Zhong, B. Q., Chang, M., Shao, M., Wang, X. M., 2022: A New Index Developed for Fast Diagnosis of Meteorological Roles in Ground-Level Ozone Variations. Adv. Atmos. Sci. 39, 403–414, https://doi.org/10.1007/s00376-021-1257-x.

Cooper, O. R., 2019: Detecting the fingerprints of observed climate change on surface ozone variability, Sci. Bull., 64, 359-360, https://doi.org/10.1016/j.scib.2019.02.013.

Copernicus Climate Change Service and Climate Data Store, 2023: ERA5 hourly data on pressure levels from 1940 to present. Copernicus Climate Change Service (C3S) Climate Data Store (CDS) [data set], https://doi.org/10.24381/cds.bd0915c6.

Cristofanelli, P., Bracci, A., Sprenger, M., Marinoni, A., Bonafè, U., Calzolari, F., Duchi, R., Laj, P., Pichon, J. M., Roccato, F., Venzac, H., Vuillermoz, E., and Bonasoni, P., 2010: Tropospheric ozone variations at the Nepal Climate

https://doi.org/10.5194/egusphere-2026-2146
Preprint. Discussion started: 4 May 2026


Observatory-Pyramid (Himalayas, 5079 m a.s.l.) and influence of deep stratospheric intrusion events, Atmos. Chem. Phys., 10, 6537-6549, https://doi.org/10.5194/acp-10-6537-2010.

Danielsen, E. F. and Mohnen, V. A., 1997: Project dustorm report: ozone transport, in situ measurements, and meteorological analyses of tropopause folding, J. Geophys. Res. (1896-1977), 82, 5867-5877, https://doi.org/https://doi.org/10.1029/JC082i037p05867.

Ding, A. J. and Wang, T., 2006: Influence of stratosphere-to-troposphere exchange on the seasonal cycle of surface ozone at Mount Waliguan in western China - art. no. L03803, Geophys. Res. Lett., 33, https://doi.org/10.1029/2005gl024760.

Duan, J., Tian, W., Zhang, J., Hu, Y., Yang, J., Wang, T., and Huang, R., 2023: Impact of the Indian Ocean SST on Wintertime Total Column Ozone Over the Tibetan Plateau, J. Geophys. Res. - Atmos., 128, https://doi.org/10.1029/2022jd037850.

Edmon, H. J., Hoskins, B. J., and McIntyre, M. E., 1980: Eliassen-Palm Cross Sections for the Troposphere, J. Atmos. Sci., 37, 2600-2616, https://doi.org/https://doi.org/10.1175/1520-0469(1980)037<2600:EPCSFT>2.0.CO;2.

Enfield, D. B. and Mayer, D., 1997: Tropical atlantic sea surface temperature variability and its relation to El Nino-Southern Oscillation, J. Geophys. Res. C: Oceans, 102, 929-945, https://doi.org/10.1029/96JC03296.

Evans, J. P. and McCabe, M. F., 2010: Regional climate simulation over Australia's Murray-Darling basin: A multitemporal assessment, J. Geophys. Res. - Atmos., 115, https://doi.org/10.1029/2010jd013816.

Gasperini, F., 2019: SD WACCM-X v2.1, NSF National Center for Atmospheric Research [data set], https://doi.org/10.26024/5b58-nc53.

Grell, G. A., Peckham, S. E., Schmitz, R., McKeen, S. A., Frost, G., Skamarock, W. C., and Eder, B., 2005: Fully coupled "online" chemistry within the WRF model, Atmos. Environ., 39, 6957-6975, https://doi.org/10.1016/j.atmosenv.2005.04.027.

Holton, J. R., Haynes, P. H., McIntyre, M. E., Douglass, A. R., Rood, R. B., and Pfister, L., 1995: Stratosphere-troposphere exchange, Rev. Geophys., 33, 403-439, https://doi.org/https://doi.org/10.1029/95RG02097.

Ji, X., Neelin, J. D., and Mechoso, C. R., 2016: Baroclinic-to-Barotropic Pathway in El Niño–Southern Oscillation Teleconnections from the Viewpoint of a Barotropic Rossby Wave Source. J. Atmos. Sci., 73, 4989–5002, https://doi.org/10.1175/JAS-D-16-0053.1.

Kendon, E. J., Roberts, N. M., Fowler, H. J., Roberts, M. J., Chan, S. C., and Senior, C. A., 2014: Heavier summer downpours with climate change revealed by weather forecast resolution model, Nat. Clim. Change, 4, 570-576, https://doi.org/10.1038/nclimate2258.

Koumoutsaris, S., Bey, I., Generoso, S., and Thouret, V., 2008: Influence of El Nino-Southern Oscillation on the interannual variability of tropospheric ozone in the northern midlatitudes, J. Geophys. Res. - Atmos., 113, https://doi.org/10.1029/2007jd009753.

Kug, J. S. and Kang, I. S., 2006: Interactive feedback between ENSO and the Indian Ocean, J. Clim., 19, 1784-1801, https://doi.org/10.1175/jcli3660.1.

Lamarque, J. F. and Hess, P. G., 1994: Cross-Tropopause Mass Exchange and Potential Vorticity Budget in a Simulated Tropopause Folding, J. Atmos. Sci., 51, 2246-2269, https://doi.org/https://doi.org/10.1175/1520-0469(1994)051<2246:CTMEAP>2.0.CO;2.

Langford, A. O., 1999: Stratosphere-troposphere exchange at the subtropical jet: Contribution to the tropospheric ozone budget at midlatitudes, Geophys. Res. Lett., 26, 2449-2452, https://doi.org/https://doi.org/10.1029/1999GL900556.

Lee, J., Butler, A. H., Albers, J. R., Wu, Y., and Lee, S. H., 2025: Impact of Sudden Stratospheric Warmings on the Stratosphere-To-Troposphere Transport of Ozone, Geophys. Res. Lett., 52, https://doi.org/10.1029/2024gl112588.

Li, D., and Bian, J. C., 2018: Case analysis and numerical simulation of convective transport process caused by Northeast Cold Vortex, Chin. J. Geophys. 61(9), 3607-3616, https://doi.org/10.6038/cjg2018L0173.

Li, Y., Feng, W., Zhou, X., Li, Y., and Chipperfield, M. P., 2024a: The impact of El Niño-Southern Oscillation on the total column ozone over the Tibetan Plateau, Atmos. Chem. Phys., 24, 8277-8293, https://doi.org/10.5194/acp-24-8277-2024.

Li, Y., Li, X., Feng, J., Zhou, Y., Wang, W., and Hou, Y., 2024b: Uncertainties of ENSO-related Regional Hadley Circulation Anomalies within Eight Reanalysis Datasets, Adv. Atmos. Sci., 41, 115-140, https://doi.org/10.1007/s00376-023-3047-0.

Luo, J., Liang, W., Xu, P., Xue, H., Zhang, M., Shang, L., and Tian, H., 2019: Seasonal Features and a Case Study of Tropopause Folds over the Tibetan Plateau, Adv. Meteorol., 2019, https://doi.org/10.1155/2019/4375123.

https://doi.org/10.5194/egusphere-2026-2146
Preprint. Discussion started: 4 May 2026


Manciu, A., Rammig, A., Krause, A., and Quesada, B. R., 2023: Impacts of land cover changes and global warming on climate in Colombia during ENSO events, Clim. Dyn., 61, 111-129, https://doi.org/10.1007/s00382-022-06545-1.

Met Office Hadley Centre., 2016: Hadley Centre sea ice and sea surface temperature data set, HadISST.2 [data set], https://www.metoffice.gov.uk/hadobs/hadisst/data/download.html.

Nie, W. and Li, M., 2022: July Mean Temperature Reconstruction for the Southern Tibetan Plateau Based on Tree-Ring Width Data during 1763-2020, Forests, 13, https://doi.org/10.3390/f13111911.

Olsen, M. A., Manney, G. L., and Liu, J., 2019: The ENSO and QBO Impact on Ozone Variability and Stratosphere-Troposphere Exchange Relative to the Subtropical Jets, J. Geophys. Res. - Atmos., 124, 7379-7392, https://doi.org/10.1029/2019jd030435.

Qian, W., Wu, K., and Liang, H., 2016: Arctic and Antarctic cells in the troposphere, Theor. Appl. Climatol., 125, 1-12, https://doi.org/10.1007/s00704-015-1485-z.

Ratna, S. B., Ratnam, J. V., Behera, S. K., Rautenbach, C. J. d., Ndarana, T., Takahashi, K., and Yamagata, T., 2014: Performance assessment of three convective parameterization schemes in WRF for downscaling summer rainfall over South Africa, Clim. Dyn., 42, 2931-2953, https://doi.org/10.1007/s00382-013-1918-2.

Skerlak, B., Sprenger, M., Pfahl, S., Tyrlis, E., and Wernli, H., 2015: Tropopause folds in ERA-Interim: Global climatology and relation to extreme weather events, J. Geophys. Res. - Atmos., 120, 4860-4877, https://doi.org/10.1002/2014jd022787.

Stohl, A., Bonasoni, P., Cristofanelli, P., Collins, W., Feichter, J., Frank, A., Forster, C., Gerasopoulos, E., Gäggeler, H., James, P., Kentarchos, T., Kromp-Kolb, H., Krüger, B., Land, C., Meloen, J., Papayannis, A., Priller, A., Seibert, P., Sprenger, M., Roelofs, G. J., Scheel, H. E., Schnabel, C., Siegmund, P., Tobler, L., Trickl, T., Wernli, H., Wirth, V., Zanis, P., and Zerefos, C., 2003: Stratosphere-troposphere exchange: A review, and what we have learned from STACCATO - art. no. 8516, J. Geophys. Res. - Atmos., 108, https://doi.org/10.1029/2002jd002490.

Sun, B., 2018: Asymmetric variations in the tropical ascending branches of Hadley circulations and the associated mechanisms and effects. Adv. Atmos. Sci. 35, 317–333, https://doi.org/10.1007/s00376-017-7089-z.

Thurairajah, B. and Cullens, C. Y., 2022: On the Downward Progression of Stratospheric Temperature Anomalies Using Long-Term SABER Observations, J. Geophys. Res. - Atmos., 127, https://doi.org/10.1029/2022jd036487.

Tian, W. S., Huang, J. L., Zhang, J. K., Xie, F., Wang, W. K., Peng, Y. F., 2023: Role of Stratospheric Processes in Climate Change: Advances and Challenges. Adv. Atmos. Sci. 40, 1379–1400, https://doi.org/10.1007/s00376-023-2341-1.

Timmermann, A., An, S. I., Kug, J. S., Jin, F. F., Cai, W., Capotondi, A., Cobb, K. M., Lengaigne, M., McPhaden, M. J., Stuecker, M. F., Stein, K., Wittenberg, A. T., Yun, K. S., Bayr, T., Chen, H. C., Chikamoto, Y., Dewitte, B., Dommenget, D., Grothe, P., Guilyardi, E., Ham, Y. G., Hayashi, M., Ineson, S., Kang, D., Kim, S., Kim, W., Lee, J. Y., Li, T., Luo, J. J., McGregor, S., Planton, Y., Power, S., Rashid, H., Ren, H. L., Santoso, A., Takahashi, K., Todd, A., Wang, G., Wang, G., Xie, R., Yang, W. H., Yeh, S. W., Yoon, J., Zeller, E., and Zhang, X., 2018: El Nino-Southern Oscillation complexity, Nature, 559, 535-545, https://doi.org/10.1038/s41586-018-0252-6.

Tyrlis, E., Skerlak, B., Sprenger, M., Wernli, H., Zittis, G., and Lelieveld, J., 2014: On the linkage between the Asian summer monsoon and tropopause fold activity over the eastern Mediterranean and the Middle East, J. Geophys. Res. - Atmos., 119, 3202-3221, https://doi.org/10.1002/2013jd021113.

von Schneidemesser, E., Monks, P. S., Allan, J. D., Bruhwiler, L., Forster, P., Fowler, D., Lauer, A., Morgan, W. T., Paasonen, P., Righi, M., Sindelarova, K., and Sutton, M. A., 2015: Chemistry and the Linkages between Air Quality and Climate Change, Chem. Rev., 115, 3856-3897, https://doi.org/10.1021/acs.chemrev.5b00089.

Voulgarakis, A., Hadjinicolaou, P., and Pyle, J. A., 2011: Increases in global tropospheric ozone following an El Nino event: examining stratospheric ozone variability as a potential driver, Atmos. Sci. Lett., 12, 228-232, https://doi.org/10.1002/asl.318.

Wang, B., Wu, R., and Fu, X., 2000: Pacific – East Asian Teleconnection: How Does ENSO Affect East Asian Climate?, J. Clim., 13, 1517-1536, https://doi.org/https://doi.org/10.1175/1520-0442(2000)013<1517:PEATHD>2.0.CO;2.

Wang, H. Y., Wang, W. K., Huang, X., and Ding, A. J., 2020: Impacts of stratosphere-to-troposphere-transport on summertime surface ozone over eastern China, Sci. Bull., 65, 276-279, https://doi.org/10.1016/j.scib.2019.11.017.

Wang, J., Li, N., Yi, W., Xue, X., Reid, I. M., Wu, J., Ye, H., Li, J., Ding, Z., Chen, J., Li, G., Tian, Y., Chang, B., Wu, J., and Zhao, L., 2024: The impact of quasi-biennial oscillation (QBO) disruptions on diurnal tides over the low- and mid-

https://doi.org/10.5194/egusphere-2026-2146
Preprint. Discussion started: 4 May 2026


latitude mesosphere and lower thermosphere (MLT) region observed by a meteor radar chain, Atmos. Chem. Phys., 24, 13299-13315, https://doi.org/10.5194/acp-24-13299-2024.

Wang, Y., Huang, G., Pan, B. X., Lin, P. F., Boers, N., Tao, W. C., Chen, Y. T., Liu, B., Li, H. J., 2024: Correcting Climate Model Sea Surface Temperature Simulations with Generative Adversarial Networks: Climatology, Interannual Variability, and Extremes. Adv. Atmos. Sci. 41, 1299–1312, https://doi.org/10.1007/s00376-024-3288-6.

Wie, J., Moon, B. K., Yeh, S. W., Park, R. J., and Kim, B. G., 2021: La Niña-related tropospheric column ozone enhancement over East Asia, Atmos. Environ., 261, 118575, https://doi.org/https://doi.org/10.1016/j.atmosenv.2021.118575.

WMO, 2022: Ozone Research and Monitoring—GAW Report No. 278, https://library.wmo.int/viewer/58360/download?file=2022OzoneAssessment.pdf&type=pdf&navigator=1.

Xie, F., Zhang, J., Li, X., Li, J., Wang, T., and Xu, M., 2020: Independent and joint influences of eastern Pacific El Nino-southern oscillation and quasi-biennial oscillation on Northern Hemispheric stratospheric ozone, Int. J. Climatol., 40, 5289-5307, https://doi.org/10.1002/joc.6519.

Xi, X. and Sokolik, I. N., 2015: Dust interannual variability and trend in Central Asia from 2000 to 2014 and their climatic linkages, J. Geophys. Res. - Atmos., 120, https://doi.org/10.1002/2015jd024092.

Xue, L., Ding, A. j., Cooper, O., Huang, X., Wang, W. K., Zhou, D. R., Wu, Z. H, McClure-Begley, A., Petropavlovskikh, I., Andreae, M. O., and Fu, C. B., 2021: ENSO and Southeast Asian biomass burning modulate subtropical trans-Pacific ozone transport, Natl. Sci. Rev., 8, https://doi.org/10.1093/nsr/nwaa132.

Yang, J. H., Kang, S. C., Hu, Y., Chen, X. T., and Rai, M., 2023: Springtime biomass burning impacts air quality and climate over the Tibetan Plateau, Atmos. Environ., 313, https://doi.org/10.1016/j.atmosenv.2023.120068.

Yin, X., Kang, S., de Foy, B., Cong, Z., Luo, J., Zhang, L., Ma, Y., Zhang, G., Rupakheti, D., and Zhang, Q., 2017: Surface ozone at Nam Co in the inland Tibetan Plateau: variation, synthesis comparison and regional representativeness, Atmos. Chem. Phys., 17, 11293-11311, https://doi.org/10.5194/acp-17-11293-2017.

Yin, X., Rupakheti, D., Zhang, G., Luo, J., Kang, S., de Foy, B., Yang, J., Ji, Z., Cong, Z., Rupakheti, M., Li, P., Hu, Y., and Zhang, Q., 2023: Surface ozone over the Tibetan Plateau controlled by stratospheric intrusion, Atmos. Chem. Phys., 23, 10137-10143, https://doi.org/10.5194/acp-23-10137-2023.

Yong, Z., Wang, Z., Xiong, J., Ye, C., Sun, H., and Wu, S., 2023: Variability in temperature extremes across the Tibetan Plateau and its non-uniform responses to different ENSO types, Clim. Change, 176, https://doi.org/10.1007/s10584-023-03566-5.

Yuan, X., Wang, Y., Li, Y., Liu, Y., Xu, W., Wang, L., and Deng, R., 2025: Impacts of ENSO on wintertime total column ozone over the Tibetan Plateau based on the historical simulations of community Earth system model, Earth Planet. Phys., 9, 424-434, https://doi.org/10.26464/epp2025006.

Yulaeva, E. and Wallace, J. M., 1994: The Signature of ENSO in Global Temperature and Precipitation Fields Derived from the Microwave Sounding Unit, J. Clim., 7, 1719-1736, https://doi.org/https://doi.org/10.1175/1520-0442(1994)007<1719:TSOEIG>2.0.CO;2.

Zeng, G. and Pyle, J. A., 2005: Influence of El Nino Southern Oscillation on stratosphere/troposphere exchange and the global tropospheric ozone budget, Geophys. Res. Lett., 32, https://doi.org/10.1029/2004gl021353.

Zhang, J., Limpasuvan, V., Orsolini, Y. J., Espy, P. J., and Hibbins, R. E., 2021: Climatological Westward-Propagating Semidiurnal Tides and Their Composite Response to Sudden Stratospheric Warmings in SuperDARN and SD-WACCM-X, J. Geophys. Res. - Atmos., 126, https://doi.org/10.1029/2020jd032895.

Zhang, J. Q., Li, D., Bian, J. C. & Bai, Z. X., 2021: Deep stratospheric intrusion and Russian wildfire induce enhanced tropospheric ozone pollution over the northern Tibetan Plateau, Atmos. Res., 259, 105662, https://doi.org/10.1016/j.atmosres.2021.105662.

Zhang, Y., Li, J., Yang, W., Du, H., Tang, X., Ye, Q., Wang, Z., Sun, Y., Pan, X., Zhu, L., and Wang, Z., 2022: Influences of stratospheric intrusions to high summer surface ozone over a heavily industrialized region in northern China, Environ. Res. Lett., 17, https://doi.org/10.1088/1748-9326/ac8b24.

Zhang, Z., Wang, Z., Liang, J., and Luo, J., 2025: Impacts of the Quasi-Biennial Oscillation and the El Niño-Southern Oscillation on Stratosphere-to-Troposphere Ozone Transport: Assessment With Chemistry-Climate Models, J. Geophys. Res. - Atmos., 130, https://doi.org/10.1029/2024jd041825.